1

East Asian Climate Change in the 21st Century as Simulated by the Coupled Climate Model ECHO-G under IPCC SRES Scenarios

Seung-Ki MIN

Meteorologisches Institut, Universität Bonn, Bonn, Germany

Stephanie LEGUTKE

Max-Planck-Institut für Meteorologie, Hamburg, Germany

Andreas HENSE

Meteorologisches Institut, Universität Bonn, Bonn, Germany

Ulrich CUBASCH

Institut für Meteorologie, Freie Universität Berlin, Berlin, Germany

Won-Tae KWON

Meteorological Research Institute, Korea Meteorological Administration, Seoul, Korea

Jae-Ho OH

Department of Environmental Atmospheric Sciences, Pukyong National University, Busan, Korea

and

Ulrich SCHLESE

Max-Planck-Institut für Meteorologie, Hamburg, Germany

(Manuscript received 9 November 2004, in final form 17 August 2005)

Abstract

Future climate changes over East Asia are studied from ensemble simulations of the coupled climate model ECHO-G, based on the Intergovernmental Panel on Climate Change (IPCC), Special Report on Emissions Scenarios (SRES) A2 and B2 scenarios. Three ensemble experiments are performed: the A2 scenario experiment with greenhouse-gas (GHG) plus sulfate aerosol forcing (referred to as A2), and the A2 and B2 scenario experiments, with GHG forcing only (A2G and B2G respectively). All experiments show that East Asian near surface temperature (T2m) and precipitation (PCP) will increase in the 21st

Corresponding author: Seung-Ki Min, Meteorologisches Institut, Universität Bonn, Auf dem Hügel 20, Bonn 53121, Germany.
E-mail: skmin@uni-bonn.de

century with larger amplitudes than global means. Seasonally varying changes are found as a larger warming in winter and fall and a stronger PCP in summer.

Relative roles of large-scale and convective precipitations (LSP and CP) are analyzed extensively. A mass flux scheme with an adjustment closure is used for cumulus parameterization. In the global mean, LSP dominates total PCP increase whereas CP controls PCP reductions near the equator in December-January-February (DJF) and 30–40°S in June-July-August (JJA). The latter originates from a weakening of the northern winter Hadley circulation and an increased static stability in the Southern Hemisphere, supporting previous results. For the East Asian mean, the CP change explains most of the increase of total PCP in JJA while the LSP change plays a more critical role in DJF. The LSP increase over the North Pacific in DJF is well associated with strengthened [weakened] baroclinicity north [south] of 40°N, i.e., a poleward shift of storm track.

Aerosol effects on East Asian climate change (A2 minus A2G patterns) are characterized by cooling and drying with patterns similar to those of the mean changes. This is inconsistent with localized features found in previous works, indicating large uncertainty in regional responses to aerosol forcing. A possible impact of GHG mitigation over the late 21st century (A2G minus B2G patterns) is more pronounced in T2m than in PCP changes, with similar patterns as in aerosol effects. Simulated CP and LSP contributions to PCP changes are insensitive to the aerosol effect as well as that of GHG mitigations.

1. Introduction

Mainly based on climate change detection and attribution results (Mitchell et al. 2001), IPCC (2001) concluded that the warming in the second half of the 20th century is largely attributable to GHG increases caused by human activities. Atmosphere-Ocean coupled General Circulation Model (AOGCM) simulations played a crucial role for this statement. They provide not only a range of internal climate variability as input to the detection and attribution studies, but also possible future projections of climate changes using emission scenarios of GHGs and aerosols (Cubasch et al. 2001). However, there still exist large uncertainties in the results of climate change detections and projections, which stem from internal climate variability, imperfection of coupled climate models, as well as from uncertainties in external forcing, emissions scenarios, and observations (IPCC 2001). The multi model ensemble (MME) approach has been widely applied as one effort to reduce the uncertainty from internal variability and inter-model difference (e.g., Giorgi and Mearns 2002; Gillett et al. 2002; Min et al. 2004). However, the MME method is limited in that its performance critically depends on that of the individual participating models. To improve the credibility of climate change projection results from the MME, it is first necessary to understand the specific characteristics of each participating model.

Several model groups have carried out future climate change simulations with their AOGCMs, using IPCC SRES A2 and B2 scenarios (model dataset available from IPCC Data Distribution Center at http://ipcc-ddc.cru.uea.ac.uk). Using seven AOGCM results, Min et al. (2004) showed that East Asia is likely to experience warmer and wetter climate over the 21st century, with stronger amplitudes than global mean changes, which supported findings of previous studies (e.g., Kitoh et al. 1997; Hu et al. 2000a, 2000b; Dai et al. 2001; Lal and Harasawa 2001; Giorgi and Mearns 2002; Buhe et al. 2003). Particularly Min et al. (2004) found large uncertainties in the future projection of regional precipitation changes which mostly arise from inter-model differences, and suggested an investigation of relative roles of convective and large-scale precipitation (CP and LSP) changes in contributing to total precipitation (PCP) changes. This might improve understanding of the mechanism of possible future changes of the East Asian summer and winter monsoon.

There have been a few studies on CP and LSP changes. Noda and Tokioka (1989) predicted an increase of global mean CP in a $2 \times CO_2$ simulation, with an atmospheric GCM coupled to a mixed layer ocean model. This result, however, is not necessarily found in fully coupled model simulations (Murphy and Mitchell 1995). Analyzing a transient 1%/yr CO_2 increase simulation with an AOGCM, Murphy and Mitchell (1995) showed that the global mean CP has increased, whereas the

convective rainfall in the Southern Hemisphere (SH) was reduced, due to an increase of static stability with a maximum near 35°S and a stronger descent of the Hadley circulation at 10°S. The increase of CP in the Northern Hemisphere (NH) showed a larger magnitude than the decrease in the SH. Brinkop (2002) found a decrease of the global mean CP in a ECHAM4/OPYC3 simulation forced by IPCC IS92 GHG scenario, however the hemispheric characteristic of the CP change was identical to that found by Murphy and Mitchell (1995): CP decreases dominantly in the SH with a larger amplitude than the CP increase in the NH. This inter-hemispheric asymmetry in CP change originates from a different warming response of both hemispheres to GHG forcing (larger surface warming in the NH than in the SH), which leads to different changes in static stability (larger in the SH than in the NH), and tropical circulation (Murphy and Mitchell 1995; Brinkop 2002). For the East Asian region, Dai et al. (2001) analyzed the NCAR CSM and PCM simulation results, based on two scenarios of a business-as-usual and a CO_2 540 ppmv stabilization case, and predicted the summer PCP increase for the East Asian monsoon region which was dominated by CP rather than LSP increase.

In this paper, we analyze future climate changes over the East Asian region from recent simulations with the AOGCM ECHO-G under IPCC SRES scenarios, focusing on near surface temperature (T2m) and PCP. Three different experiments have been simulated under GHGs and sulfate aerosol forcing. The first is three-member ensemble simulations based on A2 GHG plus aerosol scenarios, which is referred to as A2. The second and third experiments consist of two members performed with A2 and B2 GHG-only scenarios, referred to as A2G and B2G respectively. Using the simulation data, CP and LSP changes are analyzed in detail together with storm track changes over the North Pacific. In order to see whether ECHO-G results support the mechanism of CP and LSP change explained above, changes of the atmospheric meridional circulation and vertical temperature structure are analyzed. In addition, differences between A2 and A2G are used to estimate effects of aerosol forcing, which is one of the major factors in East Asian climate change (e.g., Menon et al. 2002; Qian et al. 2003). Similarly, a possible impact of GHG mitigation is assessed by searching for significant differences between A2G and B2G results in the late 21st century, assuming that we can reduce GHG emissions by the B2 scenario level from that of A2, following Min et al. (2004).

Model and experiments are described in section 2. In section 3, analysis methods are explained, together with significance tests for the difference between the experiments, and an introduction of seven other AOGCM simulations to be compared with ECHO-G. East Asian climate changes in the ECHO-G projections are described in section 4, where contributions of CP and LSP are analyzed as well as changes of the meridional circulation, zonal mean static stability, and storm tracks. Aerosol and GHG mitigation effects are also assessed. In the final section, the main findings are summarized with some discussions.

2. Model and experiments

2.1 Model description

ECHO-G consists of the atmospheric component ECHAM4, and the oceanic component HOPE-G. A general model description of ECHAM4 and of its performance in simulating the present-day climate is found in Roeckner et al. (1996). For ECHO-G, the standard ECHAM4 has been modified, such that the heat, freshwater, and momentum fluxes are calculated separately for the ice-covered and ice-free part of each grid cell following Grötzner et al. (1996), and schemes for continental river runoff, and freshwater input from glaciers, have been implemented (Legutke and Voss 1999) in order to conserve fresh water in the coupled system. Considering that HOPE-G revealed similar performance when forced with daily T30 or T42 ECHAM4 model output, the T30 version of ECHAM4 is used in order to gain computing time and enable multi ensemble simulations (Legutke et al. 1996). The vertical resolution of ECHAM4 is by 19 hybrid sigma-pressure levels, with the highest level at 10 hPa.

Total PCP in the ECHO-G model is composed of CP and LSP. LSP occurs through large-scale thermodynamic processes controlled by relative humidity (Sundqvist et al. 1989). Large-scale condensation is based on the approach of

Sundqvist (1978). CP is calculated in ECHAM4 through a mass flux scheme according to Tiedtke (1989), with an adjustment closure following Nordeng (1994) (Roeckner et al. 1996). CP is the sum of precipitations due to three types of convection: tropical deep convection, shallow cumulus convection, and mid-level convection, which are mutually exclusive (Brinkop 2002).

ECHO-G includes a tropospheric sulfur cycle model (Feichter et al. 1997) where transport, deposition, and some chemistry are calculated interactively with the atmospheric component. Dimethylsulfide (DMS), sulfur dioxide (SO_2), and sulfate aerosols (SO_4^{2-}) are the prognostic variables. It is assumed that biogenic emissions occur as DMS, whereas volcanic emissions, biomass burning, and combustion of fossil fuels occur as SO_2. Transport and diffusion of the sulfur species are treated similar to water vapor. Dry and wet depositions are parameterized by a deposition velocity and the local precipitation formation rate, respectively. DMS and SO_2 are oxidized by hydroxyl radicals (OH^-), nitrate radicals (NO_3), hydrogen peroxide (H_2O_2), and ozone (O_3), which are prescribed from estimated monthly patterns produced by a chemistry model coupled to ECHAM4 (Roelofs and Lelieveld 1995). The end product of the gaseous and aqueous oxidation of SO_2 is sulfate aerosol SO_4^{2-}, which interacts radiatively with the ECHAM4 model through direct and first-indirect effects (see Roeckner et al. 1999 for details). Note that the sulfur cycle model is switched off in the A2G and B2G simulations.

The ocean model HOPE-G is the global version of the Hamburg Ocean Primitive Equation Model (HOPE) coupled to a dynamic-thermodynamic sea ice model with snow cover included (Legutke and Maier-Reimer 1999). The horizontal resolution corresponds to a Gaussian T42 grid (about 2.8°) with meridional refinement towards the equator (of 0.5° between 10°S and 10°N), and the vertical resolution is given by 20 levels. HOPE-G has been little changed from the version described in Wolff et al. (1997) except for the thermodynamic ice growth, which is computed from the fluxes obtained from ECHAM4 rather than from internal heat-balance equations.

The coupler OASIS (Valcke et al. 2000) exchanges 10 atmospheric flux fields and four fields of ocean and sea ice surface conditions once a day. ECHO-G is flux corrected. However, unlike the usual method of flux corrections with monthly mean fluxes of heat, water, and momentum, ECHO-G flux corrections are annual mean fluxes of heat and fresh water, with no corrections for momentum flux and no variations in time. This has the advantage of not constraining seasonal variations. Also, no corrections are applied poleward of the climatological observed ice edge, which varies monthly and longitudinally according to AMIP (Atmospheric Model Intercomparison Project) sea surface temperatures (SSTs) colder than freezing point (Legutke and Voss 1999).

A more detailed description of the coupling technique of ECHO-G can be found in Legutke and Voss (1999). The climatology and internal variability of a 1000-yr control run are described in Min et al. (2005b,c). The climate variability in the 1000-yr control run has been studied in many works (e.g., Baquero-Bernal et al. 2002; Zorita et al. 2003; Rodgers et al. 2004). Recently, centennial historical and paleoclimate simulations with ECHO-G have been studied by Zorita et al. (2004), von Storch et al. (2004), and Felis et al. (2004).

2.2 Experiments and forcing

The simulations are based on IPCC SRES A2 and B2 scenarios (Nakicenovic and Swart 2000) for GHGs and sulfate aerosols. Time varying data of three main GHGs (CO_2, NH_4, and N_2O), and 16 minor GHGs including industrial chlorofluorocarbons (CFCs), hydrochlorofluorocarbons (HCFCs), and hydrofluorocarbons (HFCs) are prescribed for the period of 1860–2100. The data are based on observed concentrations for the historical period 1860–1990, while they are taken from SRES A2 and B2 scenarios for the period after 1990. Figures 1a,b,c show time series of concentrations of the three main GHGs. CO_2 concentrations increase up to 820 and 610 ppmv by 2100 in A2 and B2 respectively.

Direct and first-indirect effects of aerosols are taken into account (for details see Roeckner et al. 1999). Biogenic and volcanic sulfur emissions are kept constant with time (not shown), and anthropogenic emissions from every ten years are linearly interpolated into each year at each grid point. Figure 1e shows historical and future (A2 scenario) emissions of anthropogenic
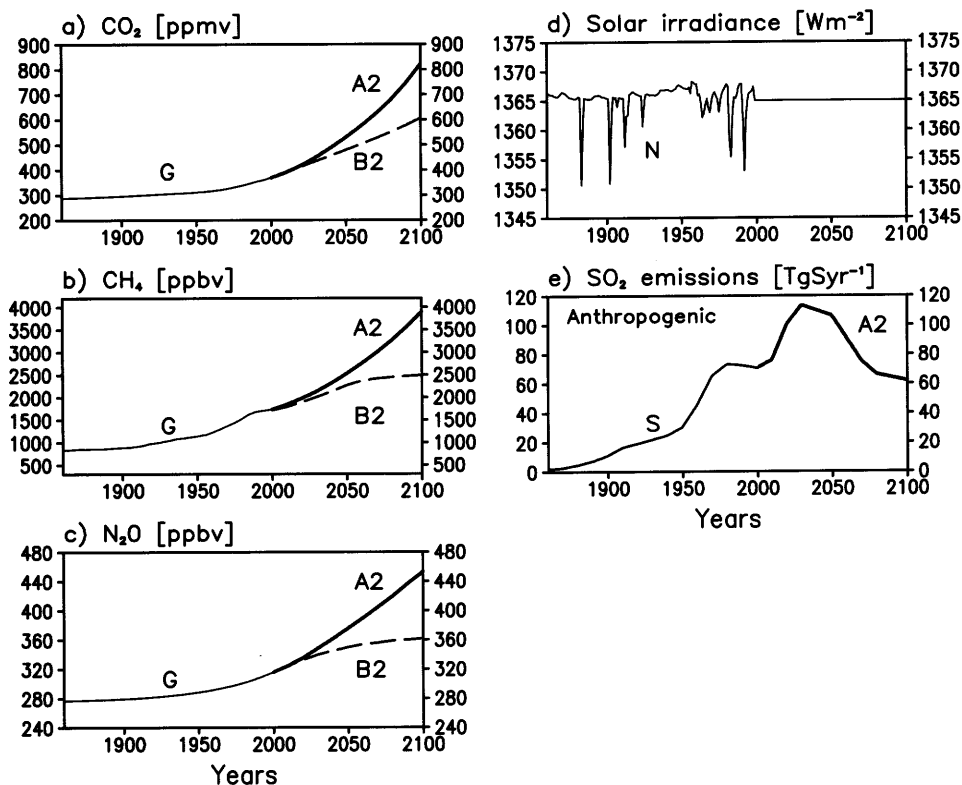
Fig. 1. Time series of external forcing used in ECHO-G simulations. Concentrations of the three major GHGs a) CO_2, b) CH_4, and c) N_2O, d) solar irradiance, and e) sulfate aerosols emissions. For GHGs and sulfate aerosols, observational data are prescribed during the period from 1860 to 1990 (denoted as G and S) while SRES A2 and B2 scenarios are specified for 1990–2100. Historical solar constant is used for 1860–1998 (denoted as N) and a constant value of 1365 W m^{-2} is given after 1999.

global SO_2. Geographical distributions of anthropogenic sulfur emissions are shown in Fig. 2 for four selected years from SRES A2. Original SRES emission data of $1° \times 1°$ resolution (Nakicenovic and Swart 2000) were interpolated into the T30 grid ($3.8° \times 3.8°$) of the atmospheric model ECHAM4, with conserving global emissions. Most emissions are found in North America and Europe in the present-day (Fig. 2a). In 2030, larger sulfur emissions are predicted in China, India, and South Africa while those from Europe and North America are reduced (Fig. 2b). In the late 21st century, emissions are reduced over most areas, as in the temporal behavior shown in Fig. 1e. Concentrations of O_3, H_2O_2, OH^-, and NO_3 are obtained by linear interpolations of available patterns in 1860 (preindustrial), 1985 (present-day), and 2050 (future), which were obtained

from Roeckner et al. (1999). Patterns of ozone and other oxidants in 2050 are based on IS92a scenario and after 2050 they are assumed constant at the 2050 values.

There are total eight realizations analyzed here. A schematic diagram of ECHO-G experiments is given in Fig. 3. Five runs have been done with ECHO-G version without aerosols: two members for both A2G (A2G_1 and A2G_2) and B2G (B2G_1 and B2G_2), and a single run for the control run (CTL). A2G and B2G runs are continuations for 1991–2100 of four member G simulations (G_1 to G_4). Hereafter we refer to the whole period simulations as G + A2G and G + B2G. Initial data for the G runs and CTL are obtained by spinning up ECHO-G for five years, starting with ocean restart files of year 310 (for G_1 + A2G_1, G_3 + B2G_1, and CTL) and 410 (for G_2 +
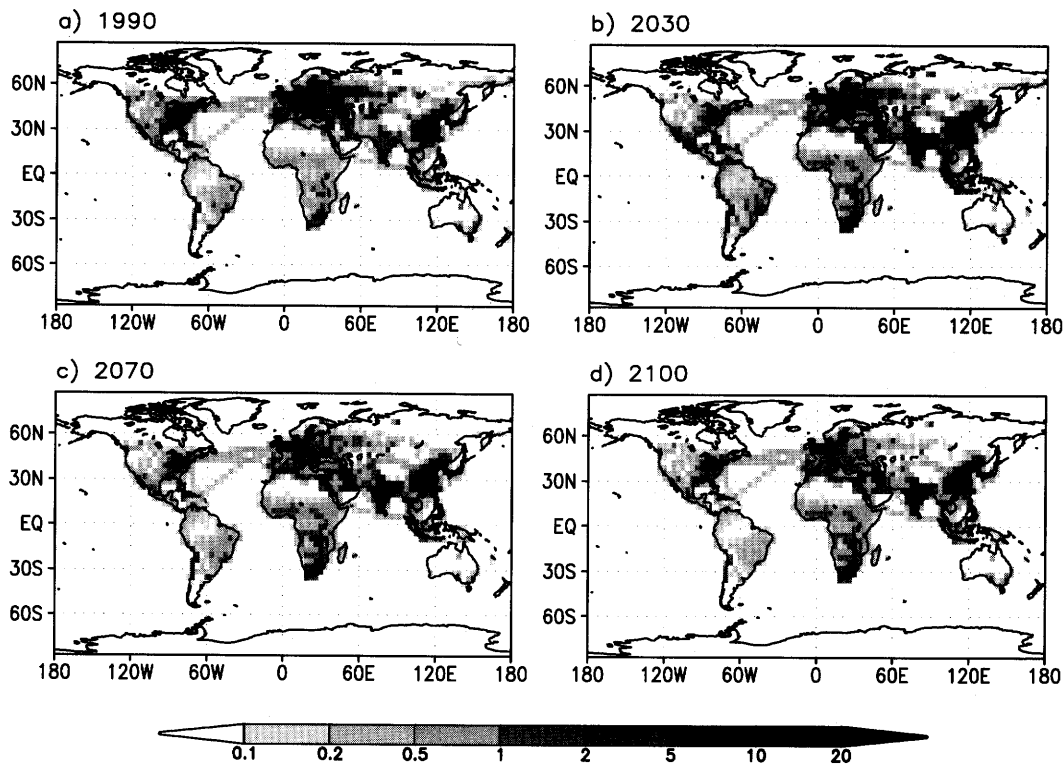
Anthropogenic Sulfur Emissions [mg m⁻² day⁻¹] SRES A2

Fig. 2. Geographical distribution of anthropogenic sulfur emissions [mg m^{-2} day^{-1}] from SRES A2 scenario for a) 1990, b) 2030, c) 2070, and d) 2100.

A2G_2 and G_4 + B2G_2) of the 1000-yr control runs, and with a climatology for ECHAM4. G_1 and G_3 [G_2 and G_4] are different from each other by taking slightly different atmospheric initial condition. The description and simple analysis results of the G_1 + A2G_1 and G_3 + B2G_1 can be found in Oh et al. (2004) and Boo et al. (2004), who dynamically downscaled East Asian climate changes using a regional climate model.

Three member A2 ensemble simulations (A2_1, A2_2, and A2_3) for the period of 2001–2100 have been carried out with the ECHO-G version including the tropospheric sulfur cycle model restarting from GSN (GHG + Sulfate aerosols + Natural forcing) historical runs (1860–2000, see Fig. 1). We refer to these simulations with aerosols for 1860–2100 as GSN + A2. Natural forcing including solar and volcanic activities is implemented through changing solar constant for 1860–1998 (Crowley 2000),

which is kept constant as 1365 W m^{-2} (historical mean for 1860–1998) from 1999 onwards. In order to get atmospheric initial conditions for the GSN runs appropriate for the interactive sulfur cycle model, a 6-year spinup of the ECHO-G aerosol version was carried out from ocean restart files of year 199, 299, and 399 of a preindustrial control run. The preindustrial control simulation was integrated by the Free University of Berlin for 576 years, with ECHO-G version without aerosols, starting from Levitus ocean climatology and atmospheric climatology of ECHAM4 as initial conditions. After a large warming trend in the first 120 years, there appears little long-term climate trend (Frank Kaspar, personal communication).

The enhancement of the three main GHG concentrations is taken into account in an appropriate way for the whole period of simulations of G_A2G and G_B2G (Roeckner et al. 1999). Because present-day daily mean atmo-
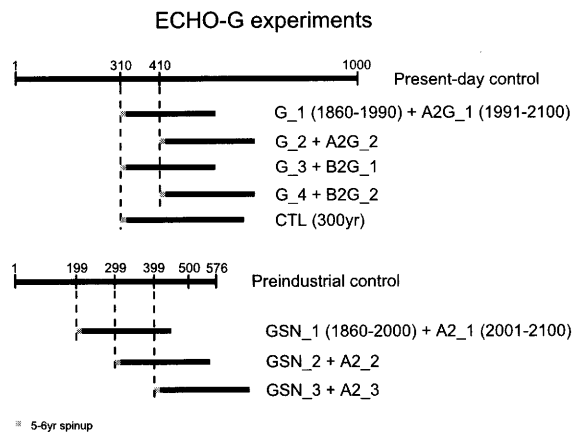
ECHO-G experiments

Fig. 3. Schematic diagram of ECHO-G experiments.

spheric fluxes (from a 15-year ECHAM4/T42 simulation with AMIP SST climatological monthly mean fields of 1979–1988) were applied for HOPE-G spin-up and flux adjustment calculation, and the 300-yr control run were performed with 1990 concentrations of the main GHGs rather than preindustrial values, the initial shift in concentrations is considered by enhancing the concentrations using a simple relationship between the radiative forcing and GHG concentrations, and keeping the radiative forcing from adjusted concentrations same as that from original concentrations (for details, see Appendix of Roeckner et al. 1999).

3. Analysis variables and methods

The analysis concentrates on T2m and PCP over East Asia, defined as the domain of 80–180°E and 20–60°N, including both land and ocean areas. Annual time series of area-averaged T2m and PCP obtained from each climate change experiments are compared, and their seasonal dependence is assessed. ECHO-G A2 results are also compared with 30-yr mean MMEs of seven AOGCMs (hereinafter referred to as MME7) from the IPCC Data Distribution Center (DDC) for three periods starting in 2010, 2040, and 2070, and with their maximum and minimum ranges (Min et al. 2004). The models are CGCM2, CCSR/NIES2, CSIRO Mk2, ECHAM4/OPYC3, GFDL_R30_c, HadCM3, and DOE PCM. The MME7 results include sulfate aerosol direct forcing (and addi-

tional aerosol indirect forcing for CCSR/NIES2, ECHAM4/OPYC3, and HadCM3, see Table 1 of Min et al. 2004) as well as GHG forcing.

To clarify a mechanism relating convection changes with changes of the Hadley circulation and static stability found in earlier studies, the atmospheric meridional circulation and vertical structures of temperature and static stability are analyzed. The meridional streamfunction (ψ) at latitude (φ) and pressure level (p) is defined as:

$$\psi(\varphi, p) = -\frac{2\pi a \cos \varphi}{g} \int_p^{p_s} [v](\varphi, p)\, dp \qquad (1)$$

where a is the radius of the Earth, g is the gravity constant, p_s is surface pressure, and $[v]$ is zonal mean meridional wind.

The static stability (S) is defined as:

$$S = \frac{T}{\theta}\frac{\partial \theta}{\partial z} = \Gamma_d - \Gamma \qquad (2)$$

where T is temperature, θ is potential temperature, Γ is the atmospheric lapse rate, and Γ_d is the dry lapse rate.

To investigate changes of storm tracks in future climate, we introduce a storm track (or baroclinicity) index following Kodama and Tamaoki (2002) and Chang (2004). The storm track index is defined as a temporal average of meridional heat flux $[v'T']$ in the lower troposphere (at 700 hPa) where the prime denotes daily deviation from monthly mean values at each grid point, and the bracket represents time average. DJF and JJA mean storm tracks over the North Pacific including East Asia are compared with changes in PCP, CP, and LSP in the late 21st century.

In order to assess aerosol effect [a potential impact of GHG mitigation], we search for statistically significant differences between A2 and A2G [A2G and B2G] results for the late 21st century. A statistical significance is tested for each grid point using univariate two-sided T-tests. Variances of two ensemble means are estimated from ten 30-yr subsections of the 300-yr CTL experiments. This is based on the assumption that the internal and intra-ensemble variability of 30-yr mean T2m and PCP will not be changed in the future by GHG and aerosol forcing. To get a more robust estimation, a strict significance level of 1% is taken for the significance test.

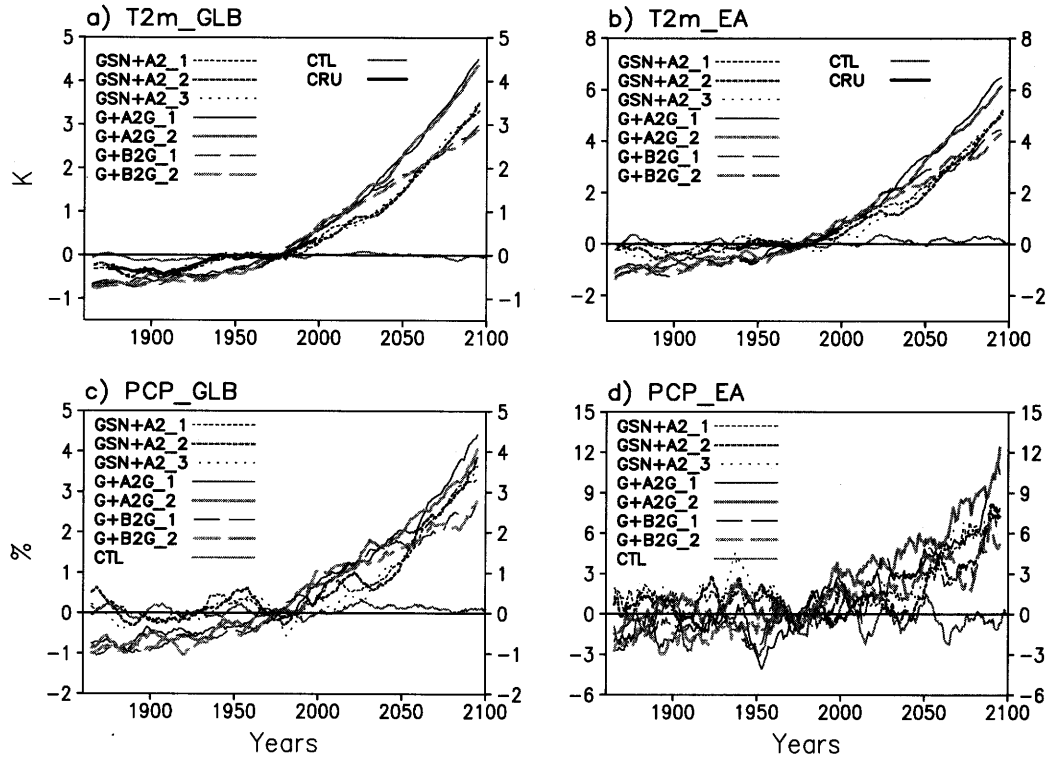Area Mean Changes Relative to 1961—1990

Fig. 4. Global and East Asian area-averaged 11-yr running mean T2m changes [K] and PCP changes [%] relative to 1961–1990 means from ECHO-G GSN + A2, G + A2G, G + B2G, and CTL experiments. CRU observations are shown together for T2m.

4. Results

4.1 Area-averaged time series

a. Temperature

Figures 4a,b show time series of 11-yr running mean global and East Asian area-averaged T2m for the ECHO-G GSN + A2, G + A2G, G + B2G, and CTL simulations. They are anomalies from the 1961–1990 mean of each simulation. The global T2m in the CTL simulation shows almost no trend, but those in the other forced simulations have positive trends ranging from 2.9–4.5 K by 2100, where the A2 warming lies between those of A2G and B2G (Fig. 4a). A kind of transient climate response (TCR), which is originally defined as "the global mean temperature change which occurs at the time of CO_2 doubling for the specific case of a 1%/yr increase of CO_2" (section 9.2.1 of Cubasch et al. 2001), can be estimated

from ECHO-G A2G and B2G runs after removing warming by non-CO_2 GHGs on the basis of different radiative forcing of non-CO_2 (1.02 W m^{-2}) and CO_2 (1.55 W m^{-2}) estimated from ECHAM4 (Table A1 of Roeckner et al. 1999). They are a bit larger than values in Table 6.11 of IPCC (2001) (0.97 and 1.46 W m^{-2} respectively), but the ratio of CO_2 [non-CO_2] radiative forcing to total GHG forcing is almost identical as 60% [40%]. The CO_2 has doubled near 2050 and 2070 in A2G and B2G (Fig. 1a). By that time, the global temperature has increased by 3.0 K in both A2G and B2G experiments (Fig. 4a), and the estimated TCR by CO_2 only, is about 60% of the warming, 1.8 K. This value is very close to TCR (1.7 K) of ECHO-G in a 1%/yr CO_2 increase experiment, which indicates a negligible effect of different warming period on T2m change (190 to 210 years versus 70 years). It is also shown in Fig. 4a that mem-

Table 1. Area-averaged T2m changes [K] in three 30-yr periods relative to 1961–1990 from SRES A2 scenario simulations with ECHO-G and the MME7 models. Values in parenthesis indicate ECHO-G A2G results without sulfate aerosol forcing. See section 3 for the list of the AOGCMs in MME7.

Model		Global mean			East Asian mean		
		2010–2039	2040–2069	2070–2099	2010–2039	2040–2069	2070–2099
ECHO-G		0.8 (1.3)	1.7 (2.5)	3.0 (3.9)	1.2 (1.8)	2.5 (3.6)	4.4 (5.5)
MME7	Mean	1.0	1.9	3.3	1.4	2.8	4.5
	Max	1.1	2.4	4.4	2.1	4.0	5.9
	Min	0.8	1.5	2.4	0.9	1.6	2.7

bers of the same scenario simulations exhibit similar responses, implying that the internal decadal variability in the global mean T2m, originating from different initial conditions, is very small compared to the difference between the scenarios. East Asian mean T2m increases have larger amplitudes than the global means ranging from 4.4–6.4 K by 2100 (Fig. 4b). The increasing trend of East Asian T2m is about 1.5 times stronger than that of global T2m. It is a general feature of AOGCM simulations that variability tends to increase with a decreasing size of the region considered. The difference between responses of ensemble members in the East Asian T2m is, however, still smaller than that between the scenarios.

Magnitudes of global and East Asian area-averaged T2m changes are listed in Table 1 for three 30-yr periods of 2020s (2010–2039), 2050s (2040–2069), and 2080s (2070–2099) in ECHO-G A2 compared with MME7 means and intra-ensemble ranges. The ECHO-G warming signal in the global and East Asia region lies close to (0.2–0.3 K less than) the MME7 mean values within the range of the seven AOGCMs. When ECHO-G A2G (values in parentheses of Table 1) is compared to ECHO-G A2, area-averaged aerosol cooling effect in the 2080s appears as −1.1 K for the East Asian region, compared to −0.9 K for the globe (see subsection 4.4).

For the historical period, T2m observations provided by the Climate Research Unit (Jones and Moberg 2003) can be compared with G and GSN simulations with ECHO-G. Observed global means are estimated for 1870–2003, while East Asian means are computed for 1933–2003, where less than 40% of the East Asian domain is void of observations (Min et al. 2005a). It is shown that the GSN simulations represent better consistencies with observational T2m changes than the G runs for the East Asia region as well as the globe, implying that observed T2m changes are attributable for both natural and anthropogenic forcing rather than only G forcing. Although a systematic analysis is needed in the comparison, which is beyond of the scope of this paper, this coincides well with previous results from other AOGCMs (IDAG 2005 and references therein).

b. Precipitation

Figures 4c,d show 11-yr running mean area-averaged PCP changes. As in the case of T2m (Fig. 4a), the forced simulations predict increasing global PCP, while the CTL simulation shows no trend. The PCP increases are about 2.8–4.3% by 2100, with A2 values positioned between A2G and B2G. ECHO-G TCR estimate for the global PCP change (60% of original PCP change by considering CO_2 only excluding contributions from non-CO_2 gases, see subsection 4.1.a) is about 1.7% [1.6%] in the A2G [B2G] experiment, which is stronger than the TCR (1.1%) in an ECHO-G 1%/yr CO_2 increase experiment. One of possible causes might be found in the longer time emission scales for the A2G and B2G experiments, compared to the 1%/yr CO_2 increase experiment. Less increase of the global PCP in the A2 experiments near

Table 2. Same as Table 1 but for PCP changes [%].

Model		Global mean			East Asian mean		
		2010–2039	2040–2069	2070–2099	2010–2039	2040–2069	2070–2099
ECHO-G		0.6 (1.3)	1.6 (2.2)	3.1 (3.6)	1.1 (3.2)	3.1 (4.8)	6.2 (8.9)
MME7	Mean	1.1	2.3	4.5	1.2	3.6	6.6
	Max	2.2	3.9	6.9	2.5	7.2	9.7
	Min	0.4	0.7	1.8	−0.0	2.0	1.4

2040s, compare to A2G and B2G can be explained by a strong effect of aerosol cooling in the period (Fig. 1e and Table 1). Although generally the PCP exhibits larger internal variability than T2m, the internal variability in the global mean PCP is smaller than the difference between the scenarios for decadal time scale. Regional PCP in East Asia shows a different behavior (Fig. 4d). First, although the A2G results appear to show larger increases than those of A2 and B2G, the internal variability is so strong that the difference between the scenarios is not clearly discernable even in the 11-yr running means. Secondly, the regional PCP changes are about 2–3 times larger than global mean changes, whereas the corresponding figure is only 1.5 for T2m changes (Figs. 4a,b).

A comparison of ECHO-G PCP changes in the A2 scenario with results from MME7 (Table 2) shows that ECHO-G predicts similar increase (0.1–0.3% less) of global and East Asian PCPs to the MME7 means. The A2 and A2G comparison shows that aerosol forcing has an effect of drying for the globe and East Asian region by −0.5 and −2.7% of PCP change respectively in the late 21st century. It is interesting to see in the subsection 4.4 that aerosol forcing implemented in this study does not have a local effect on East Asian T2m and PCP changes.

c. *Seasonal dependence*

In order to examine the seasonal dependence of climate changes, global and East Asian T2m and PCP changes in the 2080s (2070–2099) are compared between four seasons (DJF, MAM, JJA, and SON) in Fig. 5. Global mean T2m changes are 0.3–0.5 K larger in DJF and SON than in MAM and JJA in all experiments (Fig.

5a) which are statistically significant at 99% confidence level according to two-sided t test described in section 3, where variances of 30-yr seasonal mean T2m are estimated from ten (nine for DJF) 30-yr subsections of the CTL run. This stems from hemispheric differences of the land-sea distribution and different heat capacities of land and ocean. The seasonal change of East Asian temperature (Fig. 5b) shows a similar feature, but the warming in DJF becomes more prominent with values 0.8–1.1 K larger than in JJA and MAM. This supports previous results by Min et al. (2004), except that they obtained a larger warming in MAM rather than in SON. The difference comes from a different definition of the East Asia domain (100–145°E, 20–60°N) and the use of MMEs in Min et al. (2004) rather than a single model here. While Min et al. (2004) used the same regional domain as in previous studies (e.g., Giorgi and Mearns 2002; Lal and Harasawa 2001) that focused on climate change projections over land area, we take a larger domain to include oceanic area.

Global PCP increases are stronger by 0.4–1.0% in DJF and SON than in MAM and JJA (Fig. 5c), which are in general statistically significant at 99% level, similar to the finding in the global T2m response (Fig. 5a) except for two cases: difference between DJF and JJA from A2_1 and that between DJF and MAM from B2G_2. In contrast to the result for global PCP, East Asian PCP exhibits a significantly larger (>10%) increase of PCP in JJA than in other seasons, which is not consistent with the seasonal distribution of East Asian T2m change, i.e., larger winter warming. The partition of PCP into CP and LSP reveals that the stronger increase of summer PCP over East Asia is ex-
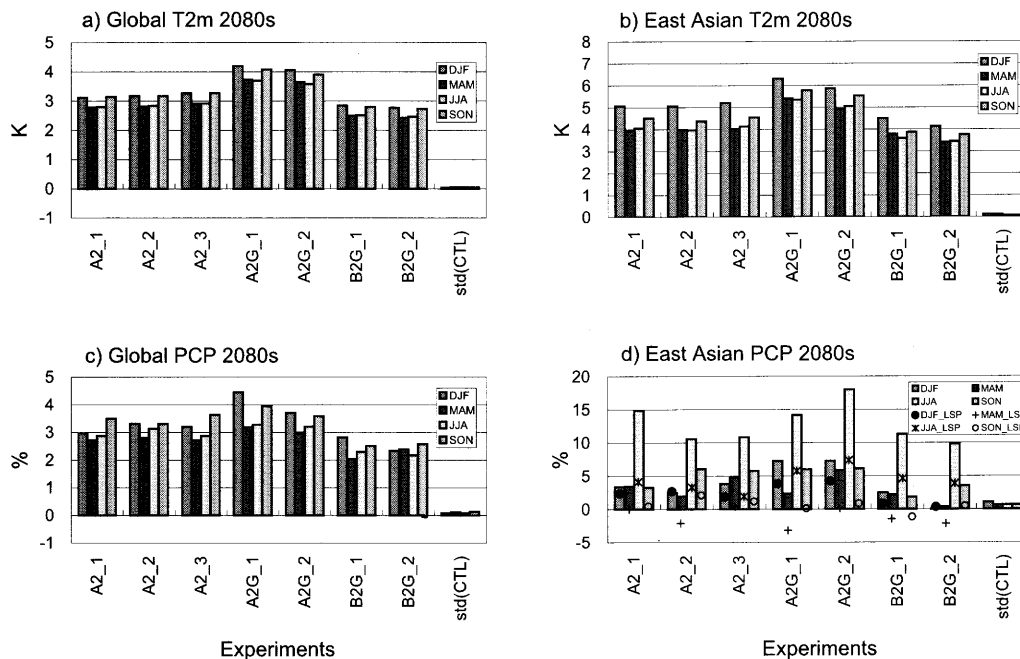
Fig. 5.   Seasonal mean changes of global and East Asian area-averaged T2m [K] and PCP [%] for the 2080s (2070–2099) relative to 1961–1990 means from ECHO-G A2, A2G, and B2G, and standard deviations (denoted as 'std') of 30-yr seasonal means estimated from CTL experiments. In d), seasonal mean changes of LSP [%] relative to the 1961–1990 mean PCP are depicted where CP contributions [%] can be estimated as PCP minus LSP changes.

plained by both CP and LSP increases (see marks in Fig. 5d). This indicates an important characteristic of simulated seasonality in regional climate change. Min et al. (2004) also found a consistent increase of East Asian summer PCP from MME7, and discussed a possible intensification of East Asian summer monsoon (Kitoh et al. 1997; Hu et al. 2000b). However, Min et al. (2004) pointed to the problematic dry biases of AOGCMs in simulating the East Asian summer climate, which reduces the reliability of the projection result. Since ECHO-G also has a dry bias in East Asian JJA PCP (Fig. 10 of Min et al. 2005b), the interpretation of summer PCP increase found here should be done with care. CP and LSP contributions to this seasonal PCP change over East Asia will be analyzed further below.

4.2   Spatial patterns
a.   Temperature
   Figures 6a,c show global patterns of DJF and JJA T2m changes in the 2080s from ECHO-G A2G experiment (mean of A2G_1 and A2G_2).

A2 and B2G patterns are similar with smaller amplitudes (not shown). The DJF global pattern is characterized by larger warming in NH high latitudes, with a maximum of 20 K near the North Pole. Warming over the ocean is less than over land, and T2m change in the Southern Ocean is near zero, which is evident in the zonal mean pattern. East Asian T2m in DJF (see the box in Fig. 6a) increase more in higher latitude continental areas than in lower latitude oceanic areas, which are the same as in other models (Min et al. 2004). T2m changes in JJA have smaller amplitudes than in DJF by 0.5 and 0.9 K for the global and East Asian means respectively (Fig. 6c). Additionally, the JJA T2m, characterized by a dominant warming in the NH mid-latitude with maximum amplitude of 10 K in the Tibetan plateau, reveals a pattern different from that in DJF.
   In the patterns of T2m change, apart from the continental warming, a notable warming appears in the Northwestern Pacific, which is seen in both DJF and JJA (Figs. 6a,c). This warming is well developed in the upper ocean
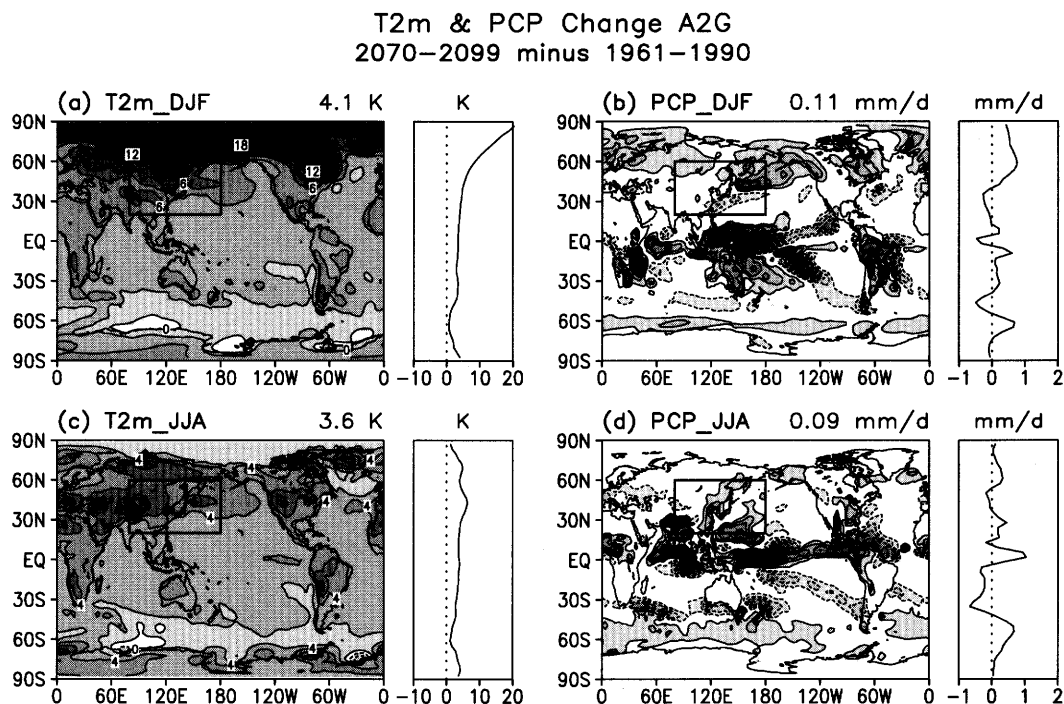
Fig. 6. Global and zonal mean patterns of DJF and JJA mean T2m [K] and PCP changes [mm day^{-1}] for 2070–2099 relative to 1961–1990 mean from the ensemble mean of the ECHO-G A2G experiments. Global mean values are depicted at the right top of each global pattern. The box depicts the East Asian area used in this study.

as well (see potential temperature at 10 m in Fig. 7). It is associated with changes of the Kuroshio Current system, and of atmospheric vorticity input. The barotropic streamfunction, which characterizes the horizontal motion of the ocean, in the 2080s of the A2G ensemble mean displays a weakening of the subtropical gyre by ca. 10 Sv (22%), and of the subpolar gyre by more then 50%, compared to 1960–89 (Fig. 7). The latter results in a reduced southward transport of cold water and causes the warming in the frontal region (see well-developed negative atmospheric heat flux over the region), together with a northward shift of the front between the two gyres (compare the zero line of present-day, and future, streamfunctions near 40°N in Fig. 7). The change pattern of the wind stress curl shows that the decrease of the strength of the subpolar gyre is caused in turn by a decrease of vorticity input north of 40°N (Fig. 7), in accord with a northeastward shifts of the Aleutian Low and jet stream (not shown) (Hu et al. 2000a). The de-

crease in the wind stress curl over the region is markedly large (about 50%) compared to the present-day value. However, this warming area is not well identified in the MME mean (e.g., Figs. 9.10d,e of Cubasch et al. 2001), and might be a specific feature of the ECHO-G model.

b. Precipitation

Figures 6b,d show global patterns of PCP changes in DJF and JJA from the A2G experiments. Larger changes in DJF and JJA PCPs are seen mainly in the tropical Pacific. While DJF PCP increases in the equatorial western Pacific (120–150°E), it decreases in the central equatorial Pacific (150°E–150°W) (Fig. 6b). Interestingly, this resembles the typical pattern of DJF PCP change during La Niña rather than El Niño events (e.g., Ropelewski and Halpert 1989; Trenberth and Caron 2000), although the simulated PCP decrease in the equatorial central Pacific is positioned more westward. JJA PCP changes show an opposite pattern in some regions, i.e., an El Niño pattern in the
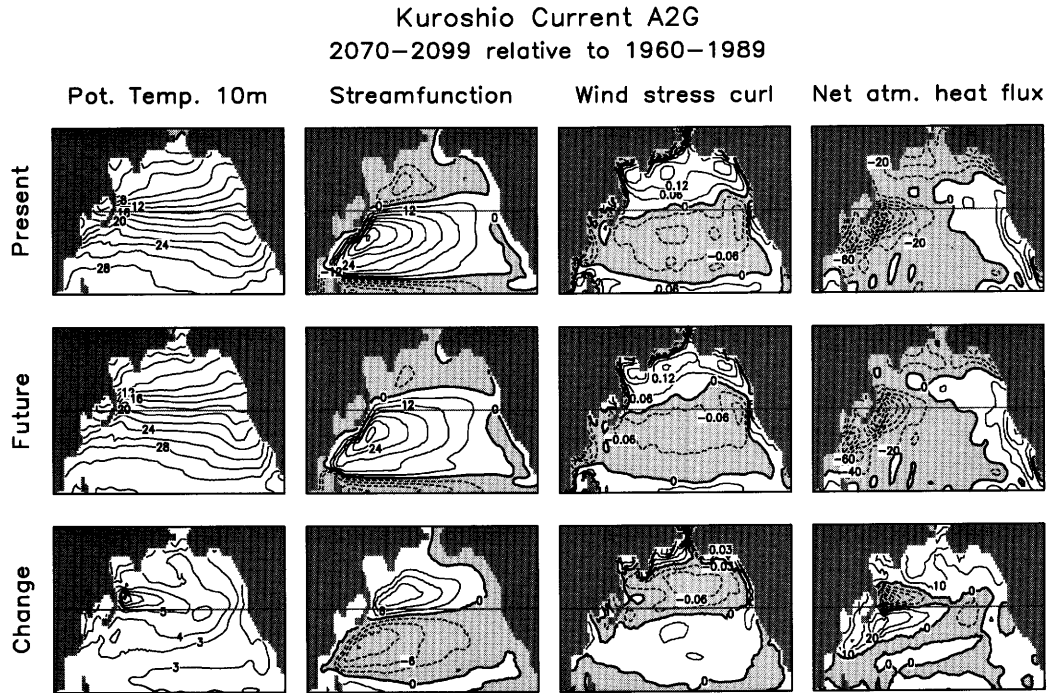
Kuroshio Current A2G
2070−2099 relative to 1960−1989

Fig. 7. Horizontal distributions of potential temperature at 10 m [K], barotropic streamfunction [m^3 s^{-1}], wind stress curl [$\times 10^6$ Pa m^{-1}], and net atmospheric heat flux over the North Pacific for present (1960–1989), future (2070–2099), and change (future–present) obtained from the A2G experiment. Negative values are dashed and shaded. Light horizontal line represents 40°N.

central tropical Pacific (Fig. 6d). However, PCP decrease is not identified in the equatorial western Pacific, instead PCP increases in the off-equatorial northwestern Pacific, equatorial Indian Ocean, and Himalayan mountain region. The changes in the last two areas appear to be related to an intensification of Indian summer monsoon (e.g., Meehl and Washington 1993; Kitoh et al. 1997; Hu et al. 2000b).

The East Asian DJF PCP change is characterized by an increase in the northwestern Pacific and a decrease in the East China Sea, while the JJA PCP change in East Asia shows an increase along the coast with a maximum near the Korean Peninsula (Figs. 6b,d; also see Figs. 13 and 14). These DJF and JJA PCP patterns, which represent possible changes of the East Asian winter and summer monsoon systems respectively, are well matched with other models (Min et al. 2004). Previous studies showed that the weakening of the East Asian winter monsoon was accompanied by a northeastward shift of the Aleutian low (Hu et al.

2000a), and that the strengthened East Asian summer monsoon was explained by an enhanced land-sea contrast and a northward shift of the convergence zone (Hu et al. 2000b; Kitoh et al. 1997). As discussed above, however, it should be noted that the reliability of the PCP pattern is not high, especially in summer, because of the low performance (dry bias) of ECHO-G in simulating the observed JJA PCP climate, which is a common error in many AOGCMs (Min et al. 2004; Giorgi and Mearns 2002). These global and East Asian characteristics in PCP changes are shared by the A2 and B2G experiments (not shown).

4.3 Convective versus large-scale precipitation changes

a. Area mean and seasonal dependence

Figure 8 shows spatial patterns of present-day climate of PCP, CP, and LSP obtained from 300-yr CTL for DJF and JJA. Simulated PCP patterns are very similar to observations as in the result of a 1000-yr control run analysis
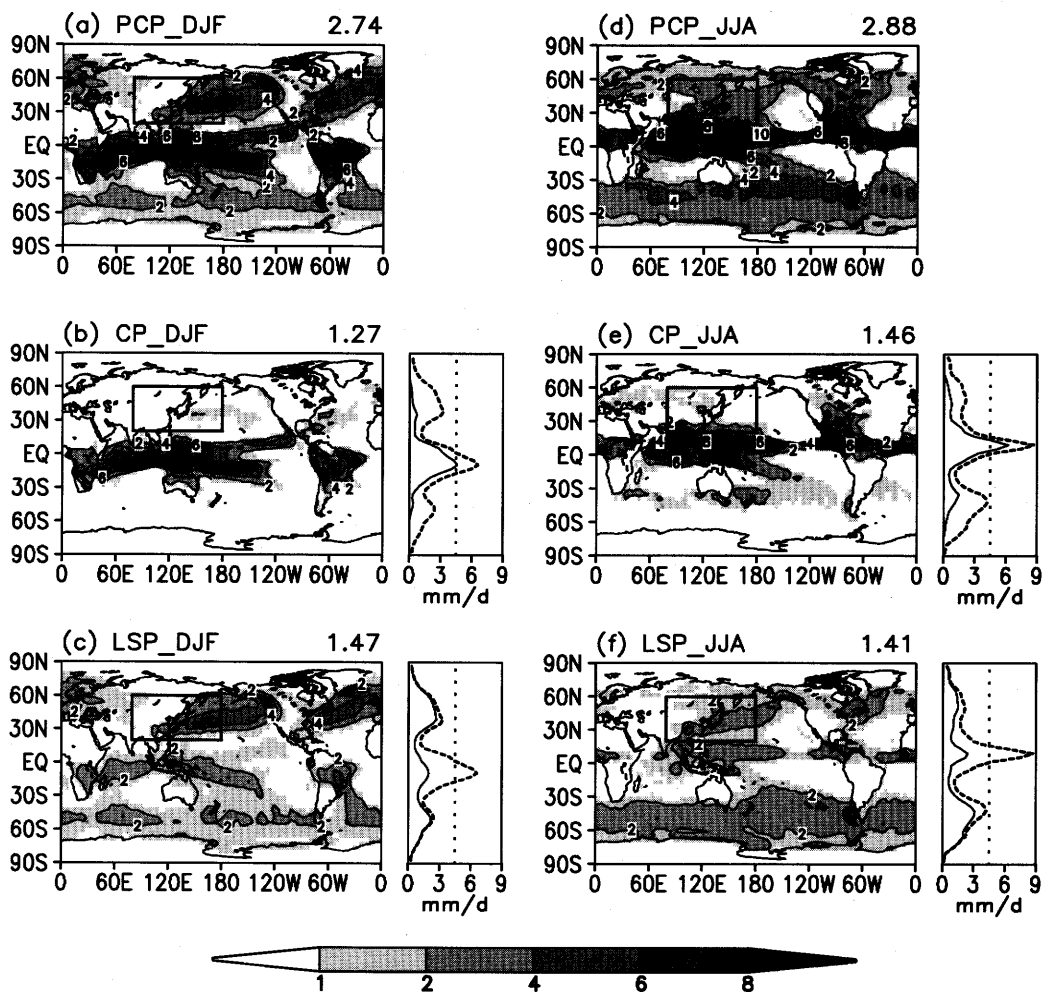
Precipitation CTL

Fig. 8.   Geographical and zonal mean distributions of present-day PCP, CP, and LSP [mm day^{-1}] patterns for DJF (left) and JJA (right) obtained from 300-yr CTL. Dashed lines represent PCP in zonal mean plots. Global mean values are depicted on the right top of each panel. The box represents the East Asian domain.

(see Fig. 9 and Fig. 10 of Min et al. 2005b). As expected, CP explains PCP mostly over the tropics, while LSP does in extratropics in accord with storm tracks (see Fig. 13), which is clearly seen in the zonal mean patterns. It is also notable that (1) larger CP is located over land area in summer hemisphere and (2) there is a certain amount of LSP (~2 mm day^{-1}) over the tropics associated with large-scale dynamics over the region. Area averaged values of present-day PCP, CP, and LSP are compared for the globe and East Asia in Table 3. Whereas the global PCP for all seasons and the East Asian PCP in JJA are explained by both CP and LSP with a contribution ratio to PCP ranging 45–54%, East Asian PCP in DJF is dominated by LSP (83%), which occurs closely related to the East Asian monsoon system.

Figure 9 shows time series of global and East Asian area-averaged CP and LSP changes from all ECHO-G experiments. Ratios of CP to PCP are analyzed together to see the relative con-

Table 3. Present-day climate values of global and East Asian mean PCP, CP, and LSP [mm day^{-1}] estimated from 300-year CTL. Values in parentheses are ratio to PCP.

Time	Global mean			East Asian mean		
	PCP	CP	LSP	PCP	CP	LSP
ANN	2.80	1.39 (0.49)	1.42 (0.51)	2.73	0.83 (0.30)	1.89 (0.70)
DJF	2.74	1.27 (0.46)	1.47 (0.54)	2.40	0.40 (0.17)	2.00 (0.83)
JJA	2.88	1.46 (0.51)	1.41 (0.49)	3.19	1.42 (0.45)	1.77 (0.55)
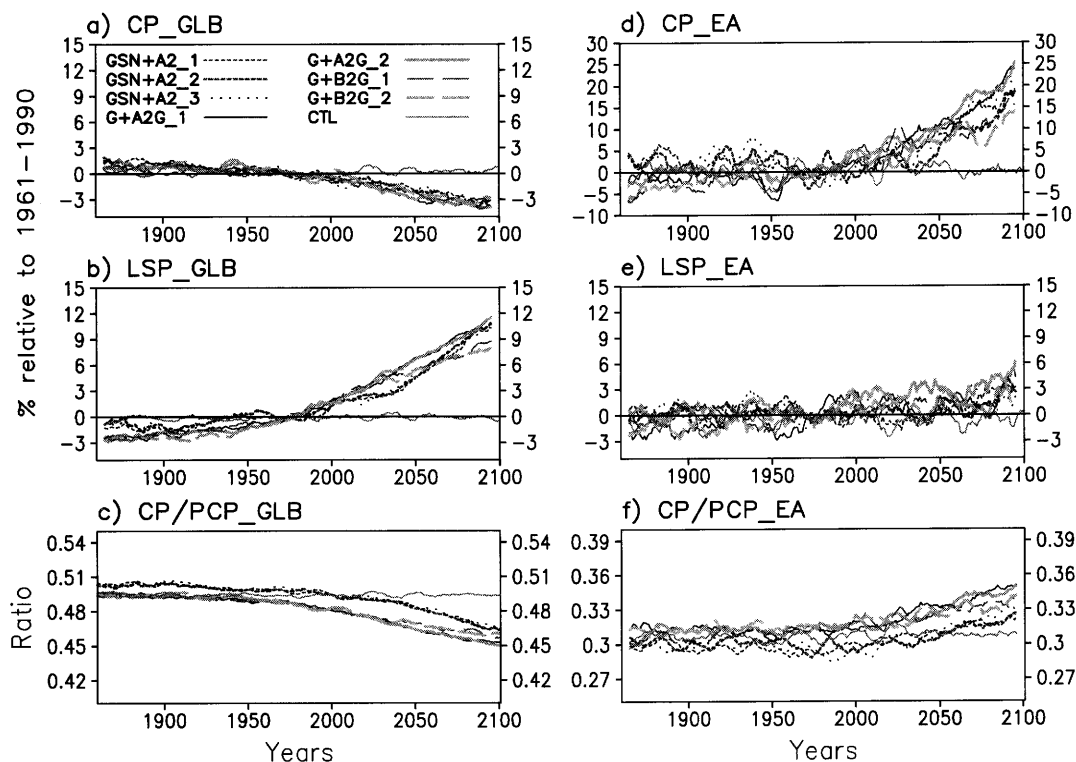
Fig. 9. Time series of global (left) and East Asian (right) area-averaged CP (top), and LSP changes (middle) [%], and ratios of CP to PCP (bottom) from the ECHO-G GSN + A2, G + A2G, G + B2G, and CTL experiments. See Table 3 for the present-day values from CTL.

tribution of CP and LSP changes to the total PCP changes. It is shown that global mean CP decreases, while global mean LSP increases in the 21st century. Since the LSP increase overwhelms the CP decrease, total PCP increases globally (Fig. 4c), consistent with the result of Brinkop (2002). Contribution ratio of CP [LSP]

to PCP also decreases [increases] by about 4% from 1860 to 2100 (Fig. 9c). It is notable that there are not significant differences between the scenarios in CP changes (Fig. 9a). On the other hand, scenario-dependent changes are clearly seen in LSP (Fig. 9b), which resemble total PCP changes in Fig. 4c. The LSP differ-
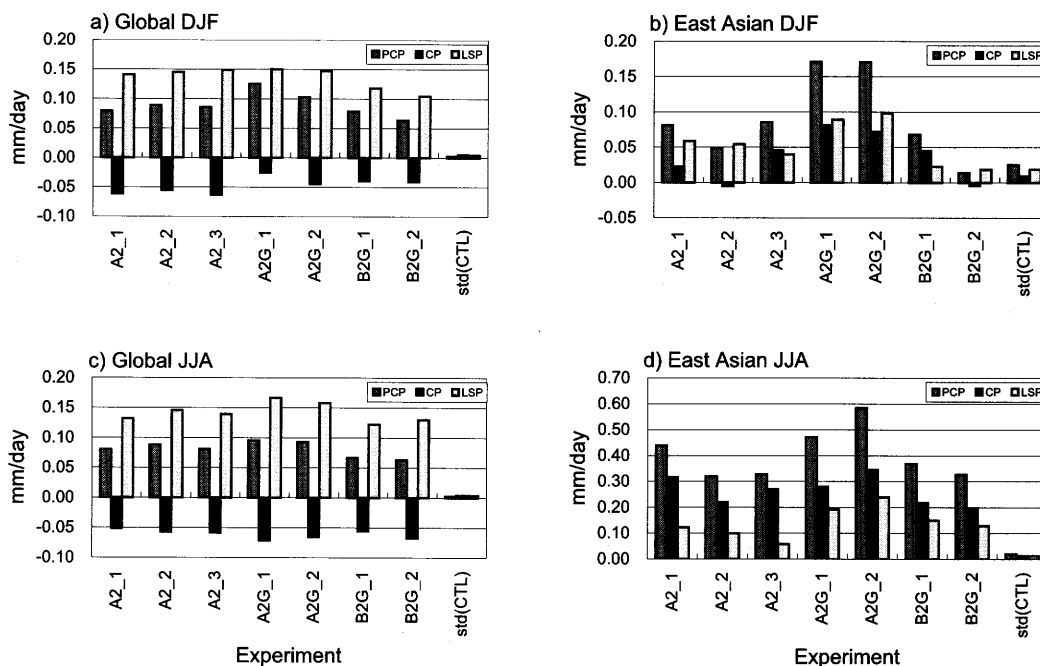
Fig. 10. DJF and JJA mean changes of global and East Asian area-averaged PCP, CP, and LSP changes [mm day^{-1}] for the 2080s (2070–2099) relative to 1961–1990 means from ECHO-G A2, A2G, and B2G experiments. Standard deviations (denoted as 'std') of 30-year seasonal means estimated from the CTL experiment are shown together for comparison. See text for a significance test of the changes.

ence in the historical period is a result of different forcing implemented, i.e., G versus GSN. A difference between the experiments can be found in the ratio of CP to PCP, which might originate from different initial climate: present day in G versus preindustrial initial conditions in GSN. However, the different initial state does not seem to affect the trends or changes.

In contrast to global mean results, both East Asian CP and LSP show increasing trends as time increases (Figs. 9d,e). The CP increase (15–25% of 1961–1990 means by 2100) is much larger than the LSP increase (2–6%). Accordingly the CP to PCP ratio over the East Asian region increases by about 3% at the end of the 21st century in all the scenario runs. Based on the satellite-driven dataset of Tropical Rainfall Measurement Mission (TRMM) Precipitation Radar (PR), Fu and Liu (2003) showed that the rain fraction ratio of convective to stratiform over the East Asia region (20–40°N, 100–140°E) is about 1:1. In comparing the CP to LSP ratio simulated by ECHO-G CTL using the

same domain, the ratios of 0.6–0.9 are found in JJA and SON, while they are as low as 0.2–0.3 in DJF and MAM, which are less than that observed by Fu and Liu (2003). However, one should keep in mind that the result by Fu and Liu (2003) is obtained from a single year, so its comparison with long-term model simulations cannot be done reasonably. In addition the definitions of CP and LSP are different between TRMM data and the model, which may be one of the reasons why the ratios are different. As in the PCP results (Fig. 4d), there are large decadal variability in East Asian CP and LSP, which makes it difficult to identify different scenarios (Figs. 9d,e).

In order to see the relative roles of CP and LSP more clearly, DJF and JJA mean changes of CP, LSP, and PCP from all members of A2, A2G, and B2G experiments are compared for the globe and East Asian region (Fig. 10). Global mean PCP increases are dominated by LSP changes in both DJF and JJA, and global mean CPs decrease consistently in all experi-
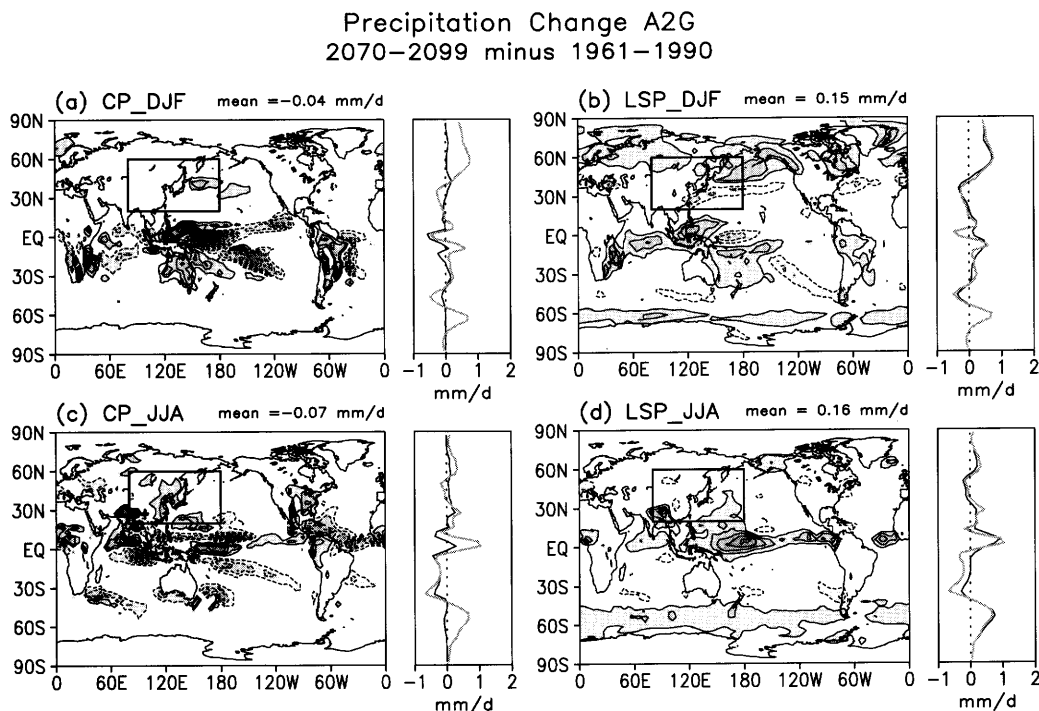
Fig. 11. Global and zonal-mean patterns of CP (left) and LSP changes (right) [mm day^{-1}] in the 2080s relative to 1961–90 from the ensemble mean of the A2G experiments. Global mean values are given at the right top of global pattern. Zero lines are omitted, contour intervals are 0.5 mm day^{-1}, and dashed contours represent negative values. The light zonal mean curves represent total PCP change. The box depicts the East Asian domain defined in this study.

ments, all of which are statistically significant at 99% confidence level (see section 3 for the *t* test). East Asian PCP increases in DJF are explained by LSP and CP together (LSP is larger in general), but JJA rainfall increases over East Asia are caused mainly by CP increases in all the simulations. A significance test shows that the PCP, CP, LSP changes over East Asia are statistically significant with respective to CTL values (near zero) at 99% confidence level in all experiments except for some variables in DJF only: CP of A2_1, CP of A2_2, LSP of B2G_1, and All variables of B2G_2. It is interesting to see that there is a marked seasonal dependence in East Asian PCP changes: PCP increases (0.32–0.58 mm day^{-1}) in JJA are more than three times of DJF PCP increases (0.01–0.17 mm day^{-1}). On the other hand, there is little difference between DJF and JJA global mean PCP changes (ratio of JJA PCP to DJF = 0.77–1.0).

b. Spatial patterns and meridional circulation changes

Figure 11 shows global distributions of DJF and JJA CP and LSP changes in the 2080s with zonal mean patterns from the A2G experiments. In the zonal means, total PCP changes are drawn together. Zonal mean patterns in Figs. 11a,c show that the CP decreases contribute to the total PCP decreases mainly near the equator in DJF and at 30–40°S in JJA, which is consistent with other model studies (Murphy and Mitchell 1995; Brinkop 2002). The meridional circulation and static stability distribution in Fig. 12 show that the equatorial CP decrease in DJF is explained by a weakening of the northern Hadley cell (compare Figs. 12a,c), while the JJA CP decreases in the SH mid latitudes occur through an increased decent (Fig. 12d) caused by an increased static stability (Fig. 12h). Such a strong increase of the static stability is not seen in the NH because of the

Meridional Circulation and Temperature Change A2G
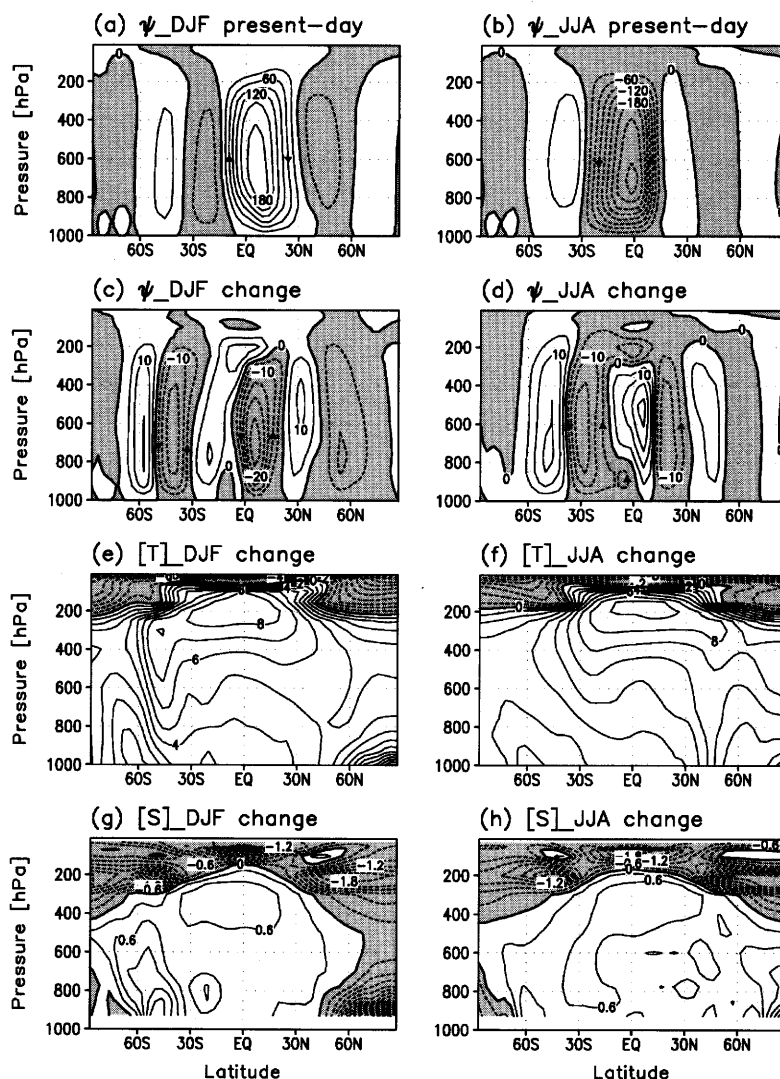2070−2099 relative to 1961−1990

Fig. 12. Vertical cross sections of DJF and JJA mean meridional stream functions [kg s^{-1}] for a), b) the present-day (1961–1990) and c), d) changes in the 2080s, e), f) zonal mean temperature changes [K] in the 2080s, and g), h) static stability changes [K km^{-1}] in the 2080s from ensemble mean A2G. Contour intervals are 30×10^9 kg s^{-1} for a) and b), 5×10^9 kg s^{-1} for c) and d), 1 K for e) and f), and 0.2 K km^{-1} for g) and h).

larger warming near the surface (Fig. 12f). Another consistent change in the stability and vertical motion can be seen near 50°S in DJF (Figs. 12c,g) where, however, SST is too cold for convection to occur. It may rather play a role in reducing LSP (Fig. 11b). An increase of CP is found over the tropical continents of the summer hemisphere (Figs. 11a,c), including the

monsoon area of India and East Asia, which is consistent overall with the T2m pattern of larger warming over land than over the ocean. Except for the two regions of zonal mean total PCP decrease explained above, the zonal mean LSP change explains most of the latitudinal change of total PCP (Figs. 11b,d). This implies that the LSP dominates the global mean PCP
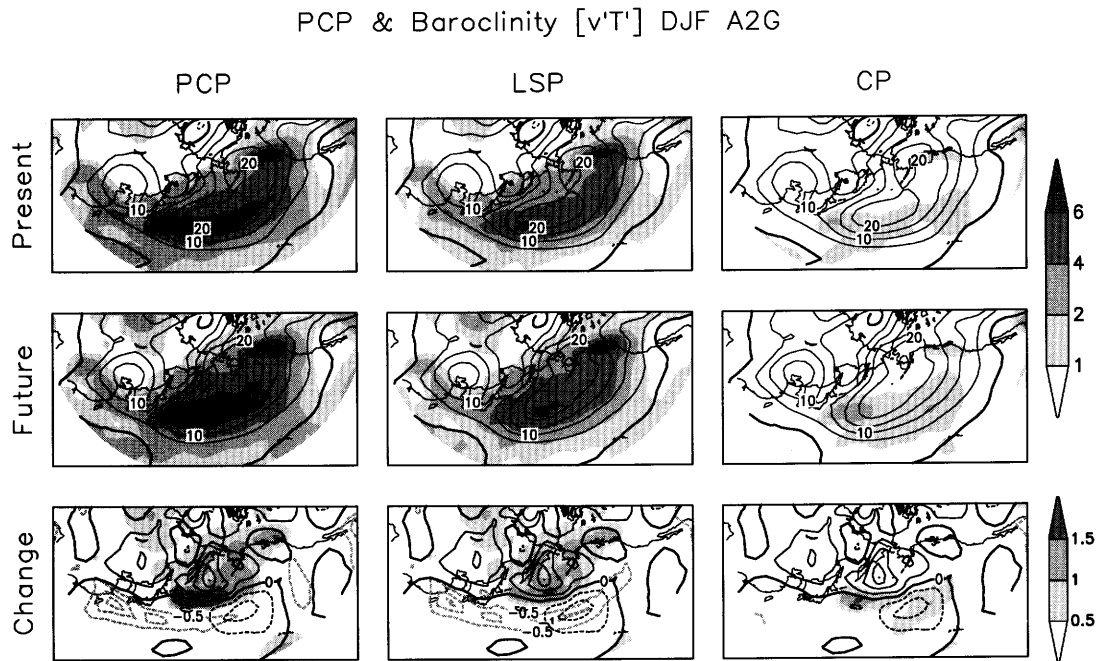
PCP & Baroclinity [v'T'] DJF A2G

Fig. 13. Horizontal patterns of present-day (1961–1990), future (2070–2099), and their difference (future–present) of DJF mean PCP, CP, LSP (shadings except for negative values in the difference plots which are represented by light dashed contours), and storm track (contour) over the North Pacific region from the A2G experiment. Storm track is defined as mean heat flux $[v'T']$. Contour intervals are 5 K m s^{-1} in present-day and future patterns, and 2 K m s^{-1} in changes. Negative contours are dashed.

changes. LSP change in JJA is somewhat remarkable in the equatorial Pacific. It might occur related to large-scale circulation change as a response of El Niño-like pattern over the region in JJA (not shown), for which further investigation is necessary.

c. Comparison with storm track changes

Wintertime CP and LSP contributions to the total PCP over East Asia are shown in Fig. 13 with present-day and future patterns, and their differences. Corresponding summertime results are shown in Fig. 14. Storm track patterns are analyzed together to see its link with LSP or CP changes. The result is based on the A2G experiment, and A2 and B2G results exhibit similar patterns with reduced amplitudes (not shown). The pattern of DJF PCP changes is controlled more by LSP change (Fig. 13). The spatial pattern of PCP and LSP change in DJF displays an increase north of, and a decrease south of 40°N, which indicates a poleward shift

of the frontal zone (Hu et al. 2000a) and the Kuroshio Current (Fig. 7). This result is in accord with storm track and baroclinicity changes (e.g., Geng and Sugi 2003 and references therein; Fischer-Bruns et al. 2005; Yin 2005). When compared with observations (e.g., Fig. 9 of Kodama and Tamaoki 2002) ECHO-G reproduces most of observed features of present-day storm tracks in DJF and JJA for the analysis region. The simulated patterns of storm tracks in DJF of present-day and future periods are well consistent with those of PCP and LSP over the North Pacific. The change of baroclinicity is characterized by a dipole around 40°N, with increase in the north and decrease in the south similar to that of PCP change, which represents a poleward shift of storm activity (Geng and Sugi 2003; Fischer-Bruns et al. 2005; Yin 2005). Yin (2005) reported a consistent response of storm track to GHG forcing from multi AOGCMs, but its mechanism is still unclear (Cubasch et al. 2001). CP increases near
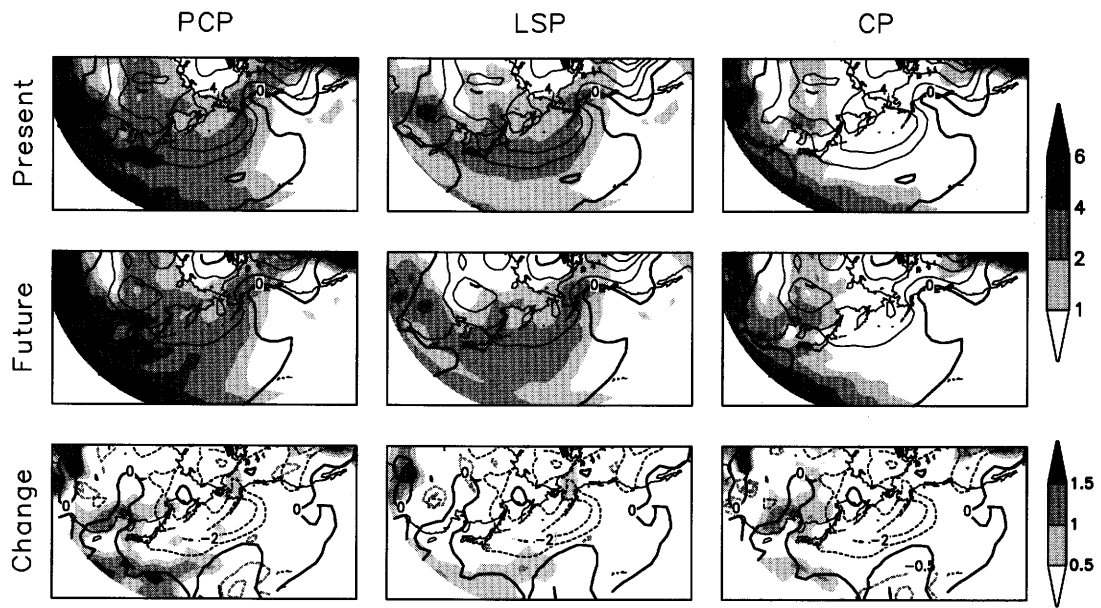
PCP & Baroclinity [v'T'] JJA A2G

Fig. 14. Same as Fig. 13 but for JJA. Contour intervals are 2 K m s^{-1} in present-day and future patterns, and 1 K m s^{-1} in differences.

the boundary of the dipole pattern, and over the southern center of baroclinicity reduction which are areas of larger SST warming (Fig. 7).

In the JJA results shown in Fig. 14, it is interesting to see that the pattern of CP change explains most of the increases in total PCP over East Asia in accord with the finding of Dai et al. (2001). Especially the increase of CP along the coastal line is well contrasted by no changes of LSP. This suggests that convection in the summer season may be a good indicator of climate changes over the East Asian region. Indeed, observational studies show an increasing frequency of extreme precipitation events in East Asia (Iwashima and Yamamoto 1993; Zhai et al. 1999; Easterling et al. 2000; Fujibe et al. 2005). Baroclinicity in JJA, which is much weaker than in DJF, is projected to decrease over the mid-latitudes with a center over the North Pacific. There is no connection between LSP and storm track changes in JJA. These results of relative dominance of CP and LSP changes and its association with storm tracks are very important, considering that these East Asian PCP changes appear consistently in many other AOGCM simulations (Giorgi and Mearns 2002; Min et al. 2004).

4.4 Aerosol versus GHG effects

There have been increasing studies of aerosol effects on East Asian climate change. From regional climate model simulations with aerosol forcing, Giorgi et al. (2002, 2003) and Qian et al. (2003) found a localized cooling effect of aerosols over China consistent with observed patterns. Comparing AOGCM experiments with and without black carbon aerosol forcing, Menon et al. (2002) argued for an important role of black carbon aerosols in East Asian climate change. However, Roeckner et al. (1999) found a widespread cooling in the NH from an AOGCM with sulfate aerosol forcing. Here, the difference between ECHO-G A2 and A2G experiments for the 2050s (2040–2069) is examined when aerosol forcing is larger (Figs. 1 and 2) to assess simulated aerosol effects on East Asian future climate. Taking a different period (e.g., 2015–2044 when maximum emissions occur over East Asia) does not change the main results. Figure 15 shows the differences
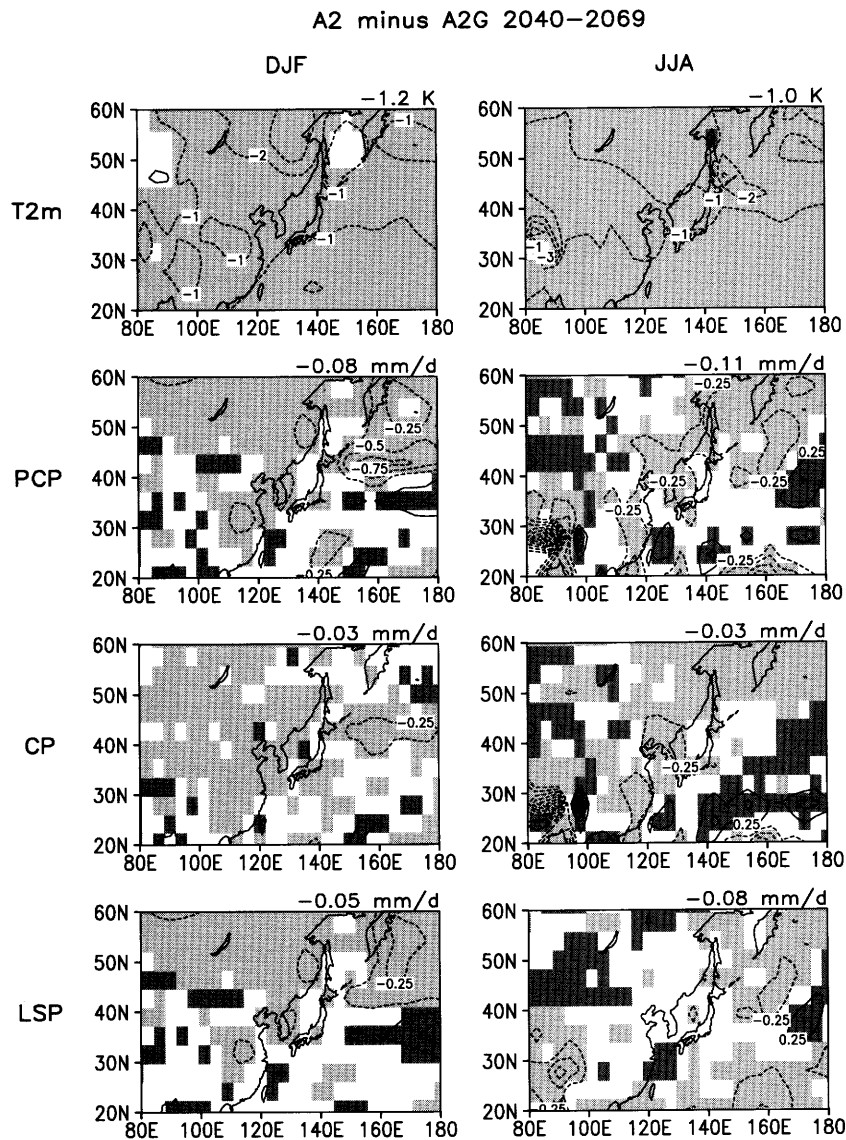
A2 minus A2G 2040-2069

Fig. 15. A2 minus A2G patterns of DJF (left) and JJA (right) mean T2m [K], PCP, CP, and LSP [mm day^{-1}] changes over East Asia in the 2050s (2040–2069) relative to 1961–1990 means. Area-averaged values are given at the right top of each panel. Dark and light shadings represent area of statistically significant positive and negative differences at 99% confidence level (see section 3 for detailed method).

for DJF and JJA mean T2m, PCP, CP and LSP. Areas of statistically significant difference are shaded (see section 3 for the method of significance test). Aerosol cooling effects can be found over large areas of East Asia with area-mean amplitudes of 1.0–1.2 K. The spatial pattern of the cooling effect resembles those of mean T2m changes in DJF and JJA (Figs. 6a,c) with oppo-

site signs. Our simulation represents little local effect of aerosols on T2m changes over the region, consistent with Roeckner et al. (1999), but unlike the other studies described above.

A2-A2G results for PCP are not well pronounced compared to the T2m results. This lower significance in PCP difference is caused by larger internal variability of PCP than of

T2m (Paeth and Hense 2002; Min et al. 2004). Aerosol effect on PCP is dominated by drying in both seasons with area-averaged values of -0.11 mm day^{-1} in JJA and -0.08 mm day^{-1} in DJF. The PCP patterns of aerosol effect look like mean change patterns of PCP changes (Figs. 6b,d) as in the T2m result. Significant reductions of PCP increase are found over the ocean north of 40°N in DJF, and over the costal region near 25–35°N in JJA, which are two marked areas of seasonal PCP increases. Similar changes by aerosol forcing are found in the LSP and CP patterns for the two areas. The former is explained by LSP decrease while the latter is by CP reduction. This confirms that sulfate aerosol forcing does not have a local impact on the simulated climate change over East Asia as in Roeckner et al. (1999). It should be noted, however, that black carbon aerosols are not included in our model simulations. Comparison with other model results indicates that there are large uncertainties arising from different models and aerosol forcing. While Qian et al. (2003) found no significant effect of sulfate and black carbon aerosols on the PCP change over East Asia, Menon et al. (2002) explained observed summer PCP increase over south China by black carbon aerosols. Considering that the two results are based on direct effect only and that the indirect effect of aerosols might be very critical (Giorgi et al. 2003), the aerosol effects on East Asian climate change needs more investigation.

Marked differences between projected patterns of A2G and B2G represent a possible impact of GHG mitigation (Min et al. 2004). It enables us to assess the extent to which the regional climate change can be diminished by reducing GHGs emissions. Figure 16 shows differences between A2G and B2G anomaly patterns for 2070–2099 over the East Asian region. Statistically significant cooling effects of GHG mitigations are found for both DJF and JJA with area means of 1.7 K. PCP results show that the area mean PCP increase can be reduced by about 0.13–0.18 mm day^{-1}. Larger areas of statistical significance, compared to the MME result of Min et al. (2004), can be explained by smaller intra-ensemble variability in a single model here. The relative roles of CP and LSP in total PCP changes by GHG mitigation effects appear the same as in the aerosol

effect (compared with Fig. 15). The local areas of significant T2m, and PCP changes, coincide well with areas of larger changes (Fig. 6), implying a spatially consistent response of East Asian climate change to different magnitudes of GHG forcing.

5. Summary and discussions

Climate change simulation results for 1860 to 2100, based on historical and IPCC SRES A2 and B2 scenarios, with the coupled AOGCM ECHO-G are analyzed focusing on the East Asian T2m and PCP. An examination of the relative contribution of CP and LSP changes to total PCP changes are highlighted, as well as storm track or baroclinicity analysis over the region. Three experiments of A2, A2G, and B2G are carried out. The A2G and B2G experiments are done with GHG forcing only, while the A2 experiment includes aerosol forcing additionally. Hence the A2 and A2G results are compared to assess aerosol effect on East Asian climate change, while the differences between A2G and B2G are used to investigate a possible impact of GHG mitigation. The main findings are summarized below with discussions.

1. All experiments predict that the East Asian climate will be warmer and wetter in the 21st century than at present, with larger amplitudes than the global means, which is consistent with previous studies (e.g., Min et al. 2004).

2. The seasonal dependence of East Asian climate change is predicted to appear as larger warming in DJF, SON and stronger rainfall in JJA, which might indicate a weakening of winter monsoon and a strengthening of summer monsoon in East Asia (Kitoh et al. 1997; Hu et al. 2000a, 2000b; Dai et al. 2001; Buhe et al. 2003; Min et al. 2004).

3. The global and East Asian PCPs are also predicted to increase. Whereas the global PCP change is explained mainly by the change of the LSP, the East Asian PCP change is dominated by CP in JJA and by LSP in DJF. LSP increase in DJF is consistent with strengthened [weakened] storm track, or baroclinicity, north [south] of 40°N, indicating a poleward shift of frontal zone (Geng and Sugi 2003; Fischer-Bruns et al. 2005; Yin 2005). However, the CP and LSP results can appear differently in other AOGCMs, depending on the parameterization
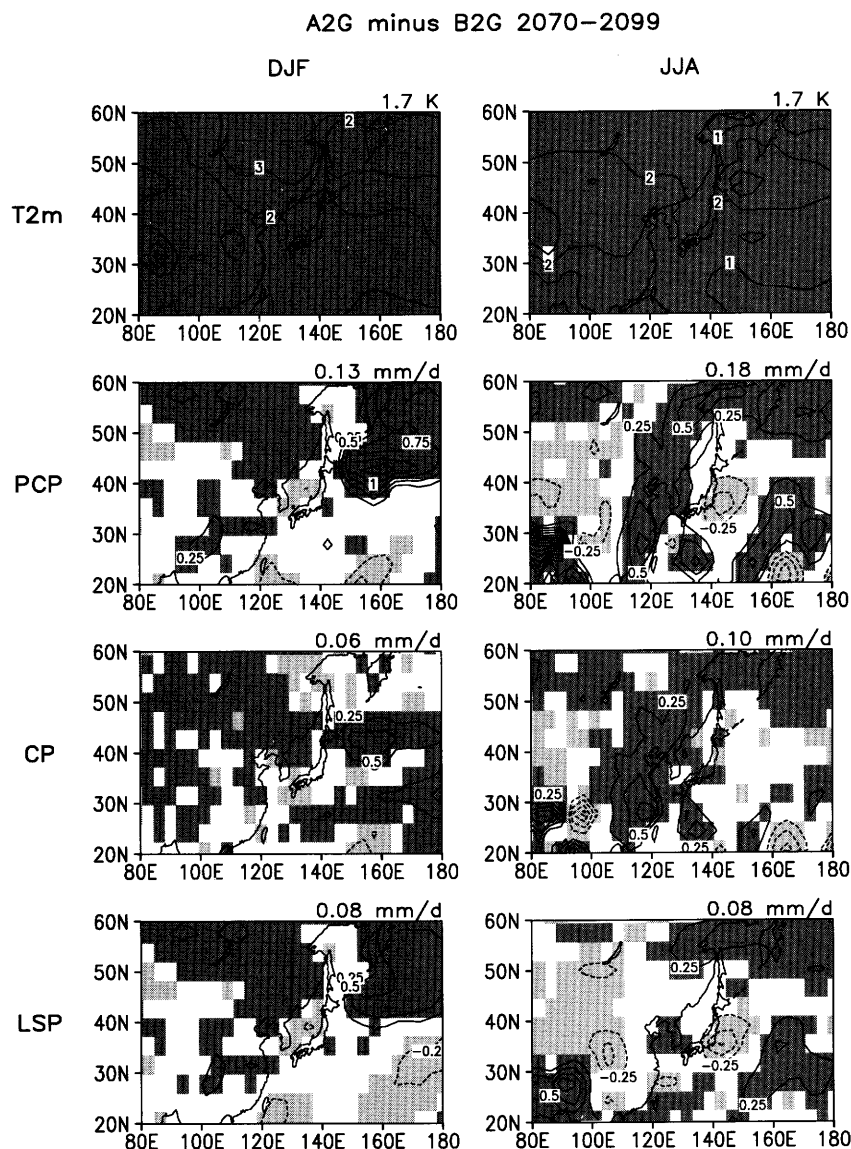
A2G minus B2G 2070-2099

Fig. 16. Same as Fig. 15 but for A2G minus B2G in the 2080s (2070–2099).

schemes and horizontal resolution (e.g., Brinkop 2002; Emori et al. 2005). In this respect, a MME approach based on the model's skill will be useful to simulate seasonal PCP patterns (Giorgi and Mearns 2002; Min et al. 2004).

4. The CP decreases near the equator in DJF and in the SH mid-latitudes in JJA are caused by a weakened northern winter Hadley circulation and an increase of static stability in the SH, respectively, which supports a mechanism suggested by previous studies (Murphy and Mitchell 1995; Brinkop 2002).

5. Spatial distributions of statistically significant aerosol effect, which are estimated from A2 minus A2G results in the mid-21st century, are characterized by a cooling over the larger part of East Asia and a drying over areas of stronger PCP increases. It is demonstrated that aerosol forcing does not change patterns of T2m changes and CP and LSP contributions to total PCP changes. This indicates that there is little local effect of sulfate aerosol forcing on simulated climate change over the region consistent with the result in Roeckner et al. (1999), but

unlike the other studies (Menon et al. 2002; Giorgi et al. 2002, 2003; Qian et al. 2003). The difference might be associated with implementations of black carbon aerosols and/or indirect effects of aerosols.

6. The potential impact of GHG mitigation, inferred from statistically significant differences between the predicted A2G and B2G climates, generally resembles those of the mean changes for T2m and PCP. The impact appears more pronounced in T2m changes than in PCP changes, which is associated with the relatively stronger internal climate variability of PCP (Paeth and Hense 2002) as in the aerosol effect.

Acknowledgements

References

Baquero-Bernal, A., M. Latif, and S. Legutke, 2002: On dipolelike variability of sea surface temperature in the tropical Indian Ocean. *J. Climate*, **15**, 1358–1368.

Boo, K.-O., W.-T. Kwon, J.-H. Oh, and H.-J. Baek, 2004: Response of global warming on regional climate change over Korea: An experiment with the MM5 model. *Geophys. Res. Lett.*, **31**, L21206, doi:10.1029/2004GL021171.

Brinkop, S., 2002: Aspects of convective activity and extreme events in a transient climate change simulation. *Meteor. Z.*, **11**, 323–333.

Buhe, C., U. Cubasch, Y. Lin, and L. Ji, 2003: The change of North China climate in transient simulations using the IPCC SRES A2 and B2 scenarios with a coupled Atmosphere-Ocean General Circulation Model. *Adv. Atmos. Sci.*, **19**, 755–766.

Chang, E.K.M., 2004: Are the Northern Hemisphere winter storm tracks significantly correlated? *J. Climate*, **17**, 4230–4244.

Crowley, T.J., 2000: Causes of climate change over the last 1000 years. *Science*, **289**, 270–277.

Cubasch, U., G.A. Meehl, G.J. Boer, R.J. Stouffer, M. Diz, A. Noda, C.A. Senior, S. Raper, and K.S. Yap, 2001: Projections of future climate change. In: *Climate Change 2001: The Scientific Basis.* Contribution of Working Group I to the Third Assessment Report of the Intergovernmental Panel on Climate Change [Houghton, J.T., Y. Ding, D.J. Griggs, M. Noguer, P.J. van der Linden, X. Dai, K. Maskell and C.A. Johnson (eds.)]. Cambridge University Press, UK, 944 pp.

Dai, A., G.A. Meehl, W.M. Washington, and T.M.L. Wigley, 2001: Climate changes in the 21st century over the Asia-Pacific region simulated by the NCAR CSM and PCM. *Adv. Atmos. Sci.*, **18**, 639–658.

Easterling, D.R., J.L. Evans, P.Ya. Groisman, T.R. Karl, K.E. Kunkel, and P. Ambenje, 2000: Observed variability and trends in extreme climate events. *Bull. Amer. Meteor. Soc.*, **81**, 417–425.

Emori, S., A. Hasegawa, T. Suzuki, and K. Dairaku, 2005: Validation, parameterization dependence, and future projection of daily precipitation simulated with a high-resolution atmospheric GCM. *Geophys. Res. Lett.*, **32**, L06708, doi:10.1029/2004GL022306.

Feichter, J., U. Lohmann, and I. Schult, 1997: The atmospheric sulfur cycle and its impact on the shortwave radiation. *Clim. Dyn.*, **13**, 235–246.

Felis, T., G. Lohmann, H. Kuhnert, S.J. Lorenz, D. Scholz, J. Pätzold, S.A. Al-Rousan, and S.M. Al-Moghrabi, 2004: Increased seasonality in Middle East temperatures during the last interglacial period. *Nature*, **429**, 164–168.

Fischer-Bruns, I., H. von Storch, F. González-Rouco, and E. Zorita, 2005: Modelling the variability of midlatitude storm activity on decadal to century time scales. *Clim. Dyn.*, **25**, 461–476.

Fu, Y. and G. Liu, 2003: Precipitation characteristics in mid-latitude East Asia as observed by TRMM PR and TMI. *J. Meteor. Soc. Japan*, **81**, 1353–1369.

Fujibe, F., N. Yamazaki, M. Katsuyama, and K. Kobayashi, 2005: The increasing trend of intense precipitation in Japan based on four-hourly data for a hundred years. *SOLA*, **1**, 041–044.

Geng, Q. and M. Sugi, 2003: Possible change of extratropical cyclone activity due to enhanced greenhouse gases and sulfate aerosols-study with a high-resolution AGCM. *J. Climate*, **16**, 2262–2274.

Gillett, N.P., F.W. Zwiers, A.J. Weaver, G.C. Hegerl, M.R. Allen, and P.A. Stott, 2002: Detecting anthropogenic influence with a multi-model

ensemble. *Geophys. Res. Lett.*, **29(20)**, 1970, doi:10.1029/2002GL015836.

Giorgi, F. and L.O. Mearns, 2002: Calculation of average, uncertainty range, and reliability of regional climate changes from AOGCM simulations via the "Reliability Ensemble Averaging" (REA) method. *J. Climate*, **15**, 1141–1158.

——, X.Q. Bi, and Y. Qian, 2002: Direct radiative forcing and regional climate effects of anthropogenic aerosols over East Asia: a regional coupled climate-chemistry/aerosol model study. *J. Geophys. Res.*, **107**, 4439, doi:10.1029/2001JD001066.

——, ——, and ——, 2003: Indirect vs. direct effects of anthropogenic sulfate on the climate of East Asia as simulated with a regional coupled climate-chemistry/aerosol model. *Clim. Change*, **58**, 345–376.

Grötzner, A., R. Sausen, and M. Claussen, 1996: The impact of sub-grid scale sea-ice inhomogeneities on the performance of the atmospheric general circulation model ECHAM3. *Clim. Dyn.*, **12**, 477–496.

Hu, Z.Z., L. Bengtsson, and K. Arpe, 2000a: Impact of global warming on the Asian winter monsoon in a coupled GCM. *J. Geophys. Res.*, **105**, 4607–4624.

——, M. Latif, E. Roeckner, and L. Bengtsson, 2000b: Intensified Asian summer monsoon and its variability in a coupled model forced by increasing greenhouse gas concentrations. *Geophys. Res. Lett.*, **27**, 2681–2684.

International ad hoc Detection and Attribution Group (IDAG), 2005: Detecting and attributing external influences on the climate system: a review of recent advances. *J. Climate*, **18**, 1291–1314.

IPCC, 2001: *Climate Change 2001: The Scientific Basis.* Contribution of Working Group I to the Third Assessment Report of the Intergovernmental Panel on Climate Change [Houghton, J.T., Y. Ding, D.J. Griggs, M. Noguer, P.J. van der Linden, X. Dai, K. Maskell and C.A. Johnson (eds.)]. Cambridge University Press, UK, 944 pp.

Iwashima, T. and R. Yamamoto, 1993: A statistical analysis of the extreme events: Long-term trend of heavy daily precipitation. *J. Meteor. Soc. Japan*, **71**, 637–640.

Jones, P.D. and A. Moberg, 2003: Hemispheric and large-scale surface air temperature variations: an extensive revision and an update to 2001. *J. Climate*, **16**, 206–223.

Kitoh, A., S. Yukimoto, A. Noda, and T. Motoi, 1997: Simulated changes in the Asian summer monsoon at times of increased atmospheric CO_2. *J. Meteor. Soc. Japan*, **75**, 1019–1031.

Kodama, Y.-M. and A. Tamaoki, 2002: A re-examination of precipitation activity in the subtropics and the mid-latitudes based on satellite-derived data. *J. Meteor. Soc. Japan*, **80**, 1261–1278.

Lal, M. and H. Harasawa, 2001: Future climate change scenarios for Asia as inferred from selected coupled atmosphere-ocean global climate models. *J. Meteor. Soc. Japan*, **79**, 219–227.

Legutke, S. and E. Maier-Reimer, 1999: Climatology of the HOPE-G global ocean general circulation model. *DKRZ Technical Report* No. 21, Deutsches Klimarechenzentrum, Hamburg, Germany, 90 pp.

—— and R. Voss, 1999: The Hamburg atmosphere-ocean coupled circulation model ECHO-G. *DKRZ Technical Report* No. 18, Deutsches Klimarechenzentrum, Hamburg, Germany, 62 pp.

——, E. Maier-Reimer, U. Cubasch, and A. Hellbach, 1996: Sensitivity of an OGCM to the resolution of atmospheric forcing data. *CAS/JSC WGNE Report*.

Meehl, G.A. and W.M. Washington, 1993: South Asian summer monsoon variability in a model with doubled atmospheric carbon dioxide concentration. *Science*, **260**, 1101–1104.

Menon, S., J. Hansen, L. Nazarenko, and Y.F. Luo, 2002: Climate effects of black carbon aerosols in China and India. *Science*, **297**, 2250–2253.

Min, S.-K., E.-H. Park, and W.-T. Kwon, 2004: Future projections of East Asian climate change from multi-AOGCM ensembles of IPCC SRES scenario simulations. *J. Meteor. Soc. Japan*, **82**, 1187–1211.

——, A. Hense, and W.-T. Kwon, 2005a: Regional-scale climate change detection using a Bayesian decision method. *Geophys. Res. Lett.*, **32**, L03706, doi:10.1029/2004GL021028.

——, S. Legutke, A. Hense, and W.-T. Kwon, 2005b: Internal variability in a 1000-year control simulation with the coupled climate model ECHO-G—I. Near-surface temperature, precipitation, and mean sea level pressure. *Tellus*, **57A**, 605–621.

——, ——, ——, and ——, 2005c: Internal variability in a 1000-year control simulation with the coupled climate model ECHO-G—II. El Niño and Southern Oscillation and North Atlantic Oscillation. *Tellus*, **57A**, 622–640.

Mitchell, J.F.B., D.J. Karoly, G.C. Hegerl, F.W. Zwiers, M.R. Allen, and J. Marengo, 2001: Detection of climate change and attribution of causes. In: *Climate Change 2001: The Scientific Basis.* Contribution of Working Group I to the Third Assessment Report of the Intergovernmental Panel on Climate Change [Houghton, J.T., Y. Ding, D.J. Griggs, M. Noguer, P.J. van

der Linden, X. Dai, K. Maskell and C.A. Johnson (eds.)]. Cambridge University Press, UK, 944 pp.

Murphy, J.M. and J.F.B. Mitchell, 1995: Transient response of the Hadley Centre coupled ocean-atmosphere model to increasing carbon dioxide. Part II: spatial and temporal structure of response. *J. Climate*, **8**, 57–80.

Nakicenovic, N. and R. Swart (eds.), 2000: *Special Report on Emissions Scenarios*. Cambridge University Press, Cambridge, UK, 612 pp.

Noda, A. and T. Tokioka, 1989: The effect of doubling the CO_2 concentration on convective and non-convective precipitation in a general circulation model coupled with a simple mixed layer ocean model. *J. Meteor. Soc. Japan*, **67**, 1057–1069.

Nordeng, T.E., 1994: Extended versions of the convective parameterization scheme at ECMWF and their impact on the mean and transient activity of the model in the tropics. ECMWF Research Department, *Technical Memorandum* No. 206, October 1994, 41 pp.

Oh, J.-H., T. Kim, M.-K. Kim, S. Lee, S.-K. Min, and W.-T. Kwon, 2004: Regional climate simulation for Korea using dynamic downscaling and statistical adjustment. *J. Meteor. Soc. Japan*, **82**, 1629–1643.

Paeth, H. and A. Hense, 2002: Sensitivity of climate change signals deduced from multi-model Monte Carlo experiments. *Clim. Res.*, **22**, 189–204.

Qian, Y., L.R. Leung, S.J. Ghan, and F. Giorgi, 2003: Regional climate effects of aerosols over China: modeling and observation. *Tellus*, **55B**, 914–934.

Rodgers, K., P. Friederichs, and M. Latif, 2004: Tropical Pacific decadal variability and its relation to decadal modulations of ENSO. *J. Climate*, **17**, 3761–3774.

Roeckner, E., K. Arpe, L. Bengtsson, M. Christoph, M. Claussen, L. Dümenil, M. Esch, M. Giorgetta, U. Schlese, and U. Schulzweida, 1996: The atmospheric general circulation model ECHAM-4: model description and simulation of present-day climate. *MPI Report* No. 218, Max Planck Institute for Meteorology, Hamburg, Germany.

———, L. Bengtsson, J. Feichter, J. Lelieveld, and H. Rodhe, 1999: Transient climate change simulations with a coupled Atmosphere-Ocean GCM including the tropospheric sulfur cycle. *J. Climate*, **12**, 3004–3032.

Roelofs, G.-J. and J. Lelieveld, 1995: Distribution and budget of O_3 in the troposphere calculated with a chemistry general circulation model. *J. Geophys. Res.*, **100**, 20983–20998.

Ropelewski, C.F. and M.S. Halpert, 1989. Precipitation patterns associated with high index phase of Southern Oscillation. *J. Climate*, **2**, 268–284.

Sundqvist, H., 1978: A parameterization scheme for non-convective condensation including prediction of cloud water content. *Quart. J. Roy. Meteor. Soc.*, **104**, 677–690.

———, E. Berge, and J.E. Kristjansson, 1989: Condensation and cloud parameterization studies with a mesoscale numerical weather prediction model. *Mon. Wea. Rev.*, **117**, 1641–1657.

Tiedtke, M., 1989: A comprehensive mass flux scheme for cumulus parameterization in large-scale models. *Mon. Wea. Rev.*, **117**, 1779–1800.

Trenberth, K.E. and J.M. Caron, 2000: The Southern Oscillation Revisited: Sea level pressures, surface temperatures and precipitation. *J. Climate*, **13**, 4358–4365.

Valcke, S., L. Terray, and A. Piacentini, 2000: The OASIS Coupler User Guide, Version 2.4, *Technical Report* TR/CMGC/00-10, CERFACS, 77 pp.

von Storch, H., E. Zorita, J. Jones, Y. Dimitriev, F. González-Rouco, and S. Tett, 2004: Reconstructing past climate from noisy data. *Science*, **306**, 679–682.

Wolff, J.-O., E. Maier-Reimer, and S. Legutke, 1997: The Hamburg Ocean Primitive Equation Model. *DKRZ Technical Report* No. 13, Deutsches Klimarechenzentrum, Hamburg, Germany, 98 pp.

Yin, J.H., 2005: A consistent poleward shift of the storm tracks in simulations of 21st century climate. *Geophys. Res. Lett.*, **32**, L18701, doi:10.1029/2005GL023684.

Zhai, P., A. Sun, F. Ren, X. Liu, B. Gao, and Q. Zhang, 1999: Changes of climate extremes in China. *Clim. Change*, **42**, 203–218.

Zorita, E., F. González-Rouco, and S. Legutke, 2003: Testing the Mann et al. (1998) approach to paleoclimate reconstructions in the context of a 1000-yr control simulation with the ECHO-G coupled climate model. *J. Climate*, **16**, 1378–1390.

———, H. von Storch, F. González-Rouco, U. Cubasch, J. Luterbacher, S. Legutke, I. Fischer-Bruns, and U. Schlese, 2004: Climate evolution in the last five centuries simulated by an atmosphere-ocean model: global temperatures, the North Atlantic Oscillation and the Late Maunder Minimum. *Meteor. Z.*, **13**, 271–289.